

# Glassy dynamics of soft matter under 1D confinement: How irreversible adsorption affects molecular packing, mobility gradients and orientational polarization in thin films

Simone Napolitano<sup>1,a</sup>, Simona Capponi<sup>2</sup>, and Bram Vanroy<sup>3</sup>

<sup>1</sup> Laboratory of Polymer and Soft Matter Dynamics, Faculté des Sciences, Université Libre de Bruxelles, Boulevard du Triomphe, Bâtiment NO, Bruxelles 1050, Belgium

<sup>2</sup> School of Physics, University College Dublin, Belfield, Dublin, Ireland

<sup>3</sup> Department of Physics and Astronomy, KULeuven, Celestijnenlaan 200D, Leuven, 3001, Belgium

Received 15 April 2013 and Received in final form 14 May 2013

Published online: 24 June 2013 – © EDP Sciences / Società Italiana di Fisica / Springer-Verlag 2013

**Abstract.** The structural dynamics of polymers and simple liquids confined at the nanometer scale has been intensively investigated in the last two decades in order to test the validity of theories on the glass transition predicting a characteristic length scale of a few nanometers. Although this goal has not yet been reached, the anomalous behavior displayed by some systems —*e.g.* thin films of polystyrene exhibit reductions of  $T_g$  exceeding 70 K and a tremendous increase in the elastic modulus— has attracted a broad community of researchers, and provided astonishing advancement of both theoretical and experimental soft matter physics. 1D confinement is achieved in thin films, which are commonly treated as systems at thermodynamic equilibrium where free surfaces and solid interfaces introduce monotonous mobility gradients, extending for several molecular sizes. Limiting the discussion to finite-size and interfacial effects implies that film thickness and surface interactions should be sufficient to univocally determine the deviation from bulk behavior. On the contrary, such an oversimplified picture, although intuitive, cannot explain phenomena like the enhancement of segmental mobility in proximity of an adsorbing interface, or the presence of long-lasting metastable states in the liquid state. Based on our recent work, we propose a new picture on the dynamics of soft matter confined in ultrathin films, focusing on non-equilibrium and on the impact of irreversibly chain adsorption on the structural relaxation. We describe the enhancement of dynamics in terms of the excess in interfacial free volume, originating from packing frustration in the adsorbed layer (Guiselin brush) at  $t^* \ll 1$ , where  $t^*$  is the ratio between the annealing time and the time scale of adsorption. Prolonged annealing at times exceeding the reptation time (usually  $t^* \gg 1$ ) induces densification, and thus reduces the deviation from bulk behavior. In this Colloquium, after reviewing the experimental approaches permitting to investigate the structural relaxation of films with one, two or no free surfaces by means of dielectric spectroscopy, we propose several methods to determine gradients of mobility in thin films, and then discuss on the unexploited potential of analyses based on the time, temperature and thickness dependence of the orientational polarization via the dielectric strength.

## 1 Introduction

Polymers and simple liquids confined in nanometer-sized geometries have been intensively investigated in the last decades, aiming both to achieve a deeper understanding of finite-size effects in soft matter and to improve the performance of nanodevices and hybrid materials [1].

From a more fundamental point of view, the interest toward the dynamics at the nanoscale is due to the assumption that glass-forming materials show deviations

from their bulk properties when confined into dimensions similar to the intrinsic length scales of the molecular relaxation processes. Different theoretical approaches provide the same order of magnitude for the temperature-dependent length scale of the glass transition,  $\xi$ , in the order of 1–5 nm. According to the model proposed by Adam and Gibbs [2] in 1965,  $\xi$  can be identified with the characteristic dimension of the cooperative rearrangement region (CRR), that is, the smallest volume inside which a transition to a different configuration can occur without requiring a correlated change outside and on its boundary.

<sup>a</sup> e-mail: [snapolit@ulb.ac.be](mailto:snapolit@ulb.ac.be)

In the framework of the Random First Order Transition theory (RFOT) [3],  $\xi$  is instead defined as the correlation length of the dynamics within solid-like regions with aperiodic crystalline structure known as “entropic droplets”. Because the droplets are spatially and morphologically distinct,  $\xi$  represents also the characteristic length scale of the dynamic heterogeneity. A similar scenario is proposed by the two-order-parameter model (TOP) [4–6] where the droplets are replaced by solid-like islands regions with medium range crystalline order (MRCO), and the concept of cooperative motion is replaced by the idea of orientational correlation among neighboring molecules, established via intermolecular bonds [7]. Despite the fundamental theoretical differences among the aforementioned models, the temperature dependence of  $\xi$  is always of the form

$$\xi(T) = \xi_0(T - T_C)^{-\nu}, \quad (1)$$

with  $0 < \nu < 1$ , and  $T_C$  a critical temperature where  $\xi$  diverges. Due to the limited number of experimental approaches capable to catch the value of  $\xi$  in bulk samples, in the last two decades, an impressive number of independent investigations has been dedicated to the characterization of changes in the material properties when the dimension is pushed down to those expected for  $\xi$ . Although the large efforts permitted to verify the presence of intrinsic dynamic length scales subjected to a temperature dependence [8] as in eq. (1), it is commonly accepted that interfacial interactions interfere with finite-size effects at length scales much larger than  $\xi$ . It is thus not yet possible to unambiguously determine the value of length scale of the glass transition. Nevertheless, the investigation of soft matter under confinement opened to a variety of new and often unexpected phenomena, which are still fascinating a large community of researchers, crossing the boundaries of disciplines like physics, chemistry, material science and engineering.

At the state of the art, different confinement geometries have been explored by several experimental techniques and mimicked by various computational approaches. Focusing on polymers, among the possible geometries, *thin films* offer versatility in the sample preparation (often achieved via spincoating of dilute solutions) and the broad tunability of both the confinement dimension (film thickness) and the interfacial interactions (substrate). In addition to that, the possibility to selectively label thin sub-layers (thickness,  $h > 10$  nm) allowed studying how interfacial interactions propagate and alter properties like diffusion of small molecules [9], glass transition temperature,  $T_g$  [10], orientational polarization [11], and physical aging [12]. Further advantages of this geometry are inherent to the zero value of its curvature, ensuring the smallest intrinsic deviations from bulk density in the confined material, a feature not present in curved spaces (*e.g.* pores, nanospheres) [13].

In ultrathin films ( $h < 200$  nm) the impact of free surfaces and interfacial layers on the static and dynamical properties of ultrathin films cannot be neglected. Films where both surfaces are in contact with air, or another

gas, or vacuum, are labeled as *freely standing*; thin layers sandwiched between solid or liquid media are instead defined as *capped*; while with *supported* we indicate the most commonly used geometry, where a film, with a free surface, is deposited onto a solid substrate. These systems cannot be considered as dynamically homogeneous: in fact, large experimental evidence confirmed the presence of a gradient of mobility, running along the confinement dimension, see sect. 4. A rough scheme of such a gradient in a supported film is provided by a trilayer model [14,15], assuming a liquid-like layer at the free (non-supported) surface, an immobilized (or reduced mobility) layer [16] at the very interface with an attractive substrate, and a bulk-like layer capped between the layers with different mobility. Regarding the dynamics, following the tri-layer model and its generalization to smoother profiles, a reduction in  $T_g$  is usually imputed to the faster dynamics introduced by the free surface [17], while the presence of an adsorbing interface is considered as a source of slower molecular motion [12].

Such a picture, although very intuitive, fails in describing the peculiar behavior of macromolecules under confinement. Exotic phenomena like the enhancement of segmental mobility in proximity of an adsorbing interface [18, 19], the impact of solvent on the structure and the morphology of the films [20–22], or the presence of long-lasting metastable states in the glassy dynamics of thin films [23–25], cannot be explained in terms of models based on equilibrium properties and oversimplified monotonous gradient in mobility. Moreover, Glynos *et al.* [26–28] have recently verified that, due to entropic reasons, the free surface can have a  $T_g$  higher than in bulk, as for example in the case of star-shaped polymers of large functionality and low molecular weight of the arms. It is thus clear that the fast surface dynamics observed in linear polystyrene (PS) [17,29], poly(methyl methacrylate) (PMMA) [30] and other low-molecular-weight glassformers [31] is not a universal feature of soft matter dynamics.

Restricting the discussion to arguments of finite-size and interfacial effects, film thickness and surface interactions should be sufficient to univocally determine the deviation from bulk behavior in ultrathin polymer films. On the contrary, we verified that capped films of constant thickness, in contact with the same supporting medium, and annealed for times much longer than the reptation time (longest relaxation time in a bulk melt) can exhibit different  $T_g$ 's [18]. Similar results were extended by Nguyen *et al.* to supported films deposited onto a larger number of different substrates [32]. These findings are in line with recent models [33,34] suggesting that a third key parameter, namely the interfacial free volume, should also be considered.

In this Colloquium, we provide an introduction to the main issues in the glassy dynamics of ultrathin layers of soft matter, summarizing the most relevant results we obtained in the last years, and focusing on the impact of irreversible chain adsorption on the segmental dynamics.

The following text is organized in different sections. First we describe the phenomenology of the glass transition, the use of dielectric spectroscopy to investigate

the structural (segmental) dynamics, and the experimental methods to study the dielectric relaxation in ultrathin films (sect. 1) Then we discuss on the impact of nanoscopic confinement and chain adsorption on the orientational polarization (sect. 2) and the scaling of the structural relaxation in proximity of a solid interface (sect. 3). We continue with a description of several methods to evaluate gradients of molecular mobility and of thermal expansion in proximity of free surfaces and interfaces (sect. 4), and we conclude with a series of open questions on unsolved problems on the glassy dynamics of soft matter thin films (sect. 5).

### 1.1 The glass transition and the theory of dielectric polarization

Viscoelasticity is an intrinsic property of liquids and amorphous solids, those materials, in fact, respond elastically on short time scales while they flow on longer time scales. Maxwell proposed a quantitative expression for the characteristic (or structural) time  $\tau$  separating the solid and the liquid behavior, in terms of experimentally accessible quantities [35]

$$\tau = \frac{\eta}{G_{\infty}}, \quad (2)$$

where  $\eta$  is the shear viscosity and  $G_{\infty}$  the instantaneous shear modulus. Systems with a characteristic time smaller than a given observation time are considered as liquids. Vice versa, those systems where  $\tau$  exceeds the observation time are regarded as solids. At room temperature, the value of  $\tau$  for water is on the order of 10 picoseconds, consequently, on the time scale of human life, water appears as a liquid.

If cooled fast enough so that crystallization is avoided, each system can be maintained in the liquid state below its melting point [13, 36]. In this regime (supercooled state), a modest reduction of the temperature leads to an abrupt but continuous increase in the viscosity and,  $G_{\infty}$  being almost temperature independent, to a similar tremendous augment in  $\tau$ . When the characteristic time becomes so large that the liquid fails to equilibrate on the experimental time scale, the system vitrifies, undergoing the glass transition [4, 13, 36–40]. Though far from being totally understood, such a phase transition is definitely the most fascinating of the unsolved problems of condensed matter.

A direct way to measure the characteristic time  $\tau$  is given by relaxation (and retardation) experiments [41]: after the application of an external perturbation, the system requires a time  $\tau_R$  to relax toward a new equilibrium state. In the linear response regime, the response of the system to an external excitation originates from the same molecular mechanism as its spontaneous fluctuations, as assured by the fluctuations-dissipation theorem (FDT). Under these conditions the relation  $\tau_R \equiv \tau$  holds.

Proven the equivalence between different time excitation schemes, it is possible to extend the observation previously made from the time to the frequency domain. When a material is probed at an angular frequency much bigger than the inverse of its characteristic time ( $\omega\tau \gg 1$ ) a

solid-like response is obtained; vice versa, a low frequency investigation ( $\omega\tau \ll 1$ ) will provide information about the viscous behavior. We will refer to the relaxation modes related to the structural response as  $\alpha$ -modes and the related process as  $\alpha$ -, structural, or segmental (valid only in case of polymers) relaxation process [13, 42].

By means of dielectric spectroscopy, the principal measuring technique in this work, we can monitor the changes in the relaxation time of polar and non-polar systems over more than ten frequency decades [41]. In the time domain, the basic principle of the technique is the measurement of the response of the system to a perturbation described by an infinitely short electric pulse. The response of the material originates from the correlated fluctuations of permanent dipole moments, which provide the physical link between the molecular motions and the interactions with an external electrical field. Consequently, via the FDT, we correlate the time dependence of the dielectric function,  $\varepsilon(t)$ , with the time dependence of the fluctuations in polarization function coupling with the spontaneous fluctuations of the system,  $\mu(t)$ ,

$$\frac{\partial \varepsilon}{\partial t} = -\frac{1}{k_B T} \frac{\partial}{\partial t} \langle \mu(t)\mu(0) \rangle, \quad (3)$$

where  $k_B$  is the Boltzmann constant, and  $\langle \rangle$  indicates a statistically averaged function.

In an isothermal representation in the frequency domain (considering the broad range accessible, the logarithm of the frequency  $f$  is instead used), the real part of the dielectric function  $\varepsilon'(\omega)$ , often indicated as dielectric constant, drops in intensity; at high frequencies, in fact, the solid-like response lacks the orientational polarization contributions present in the liquid state, and thus probed only at lower frequencies. The inflection point in the dielectric constant, correlated via a Hilbert transformation to the maximum of the loss peak,  $f_{\max}$  is related to  $\tau$  via the relation  $2\pi f_{\max}\tau = 1$ .

The structural relaxation of polymer chains originates from the correlated motions of a limited number of repeating units [43]. The first and the last segment involved in the process must assume the same conformational state both at the beginning and at the end of the correlated motions. For isolated chains it was suggested that the segmental motion can be treated as a damped diffusion of conformational states along the chain [44].

The relaxation model here proposed is rather simple: once spontaneously generated, a conformational change would perturb bond lengths and angles. This mechanism would enhance the probability for the adjacent segments to undergo a similar transition. The damping character of the mechanism would derive from the selective nature of correlated conformational changes.

Models developed for dilute solutions of polymer chains may be extended to bulk system; similarly to isolated chains, in dense systems, in fact, *trans/gauche* transitions result in rotational fluctuations of dipoles over the chain where the dipole itself is rigidly attached [43]. In dense polymer systems, such as concentrated solutions or bulk melts, the probability that the dipoles of different chains

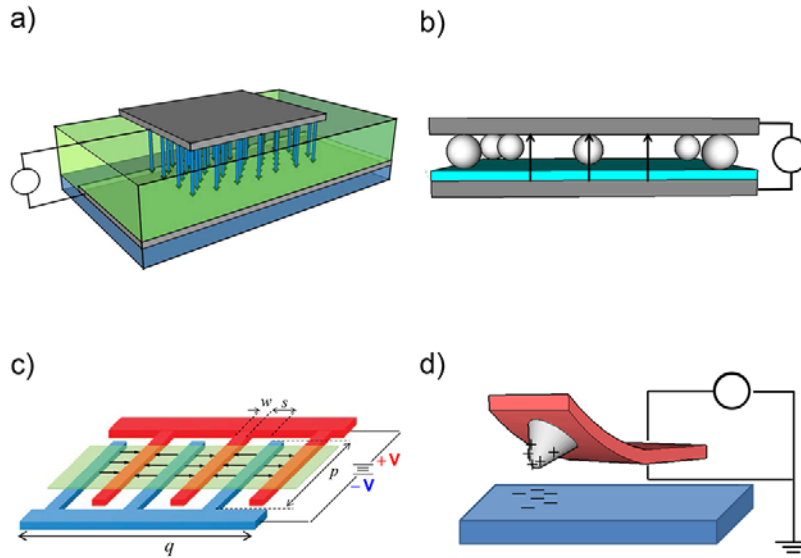


**Fig. 1.** Sketch of the approaches currently used to perform dielectric spectroscopy on ultrathin films: a) Films capped between two conductive layers. b) Supported films deposited onto a conductive layer separated from the upper electrode via nanospacers. c) Interdigitated comb electrodes (IDE). d) Local dielectric spectroscopy (LDS).

are orientationally correlated is high. In these cases, both intramolecular and intermolecular cooperativity should be taken into account. As regarding the dielectric signal, in fact, the polarization  $P$ , corresponding to the dipole density in a volume  $V_m$ , is given by

$$P = \frac{1}{V_m} \sum_{\text{chain}} \sum_{\text{repeating unit}} \mu_i, \quad (4)$$

where  $\mu_i$  is the mean dipole moment in the repeating unit  $i$ . Equation (4) can be then further expanded by considering the different contributions due to self-correlations and to cross-correlations within dipoles of different repeating units

$$\langle \mu^2 \rangle = \sum_{i=1}^N \langle \mu_i^2 \rangle + 2 \sum_{i=1}^N \sum_{j<i}^N \langle \mu_i \mu_j \rangle. \quad (5)$$

As a result from the model, a characteristic time linked to the conformational transition is related to  $\tau_\alpha$ , the relaxation time of the  $\alpha$ -process.

From numerous experimental work it results that the structural relaxation time has non-Arrhenius temperature dependence [13]: the apparent activation energy of the process increases upon cooling and shows a typical behavior that can be well described by the Vogel-Fulcher-Tammann (VFT) [45–47] empirical equation

$$\tau = \tau_\infty \exp\left(\frac{E_a(T)}{k_B T}\right) = \tau_\infty \exp\left(\frac{B T_0}{T - T_0}\right), \quad (6)$$

where  $T_0$  is the Vogel temperature,  $B$  a positive parameter related to the fragility of the system,  $E_a$  the temperature-dependent apparent activation energy and  $\tau_\infty$  the high-temperature limiting value of the relaxation time, related to the inverse of the phonon frequency. The value of  $\tau_\infty$  is on the order of  $10^{-11}$ – $10^{-15}$  s, while  $T_0$ , which corresponds

to the temperature where the relaxation time would diverge, is usually 30–70 K below the calorimetric  $T_g$ .

To extract quantitative information, isothermal dielectric spectra were analyzed by the empirical Havriliak-Negami (HN) function [48]

$$\varepsilon(\omega) = \varepsilon_\infty + \frac{\Delta\varepsilon}{[1 + (i\omega\tau_{\text{HN}})^a]^b} - i \frac{\sigma_C}{\varepsilon_0 \omega}, \quad (7)$$

where  $\varepsilon_\infty$  is the value of the dielectric constant in the absence of polarization processes (low temperature and high frequencies limit),  $\Delta\varepsilon$ ,  $\tau_{\text{HN}}$ ,  $a$ ,  $b$  indicate the dielectric strength, relaxation time and shape parameters related to the width and the asymmetry of the loss curves, respectively. Contributions to the loss signal due to ionic conductivity were taken into account by adding the term on the right, with  $\varepsilon_0$  being the vacuum permittivity.

## 1.2 Investigating the segmental dynamics under confinement via broadband dielectric spectroscopy

In the last decade different experimental approaches have been introduced to investigate the structural relaxation dynamics in ultrathin films by dielectric spectroscopy. The major technological challenge was represented by the design of the cells capable to apply a difference of voltage to films placed between electrodes, whose distance is reduced down to a few nanometers. On the other hand, the dramatic reduction of the probed volume of material required a remarkable improvement in the sensitivity of the instrumentation, and the reduction of eddy currents. In the following sections we present a short overview of the different techniques presently available, schemed in fig. 1.

### 1.2.1 Nanocapacitors (capped films)

The easiest method to apply an  $E$ -field to a polymer film (dielectric medium) is the metallization of its two surfaces, yielding to a nanocapacitor [11]. The preparation of these nanometer-spaced electrodes is started via the deposition of a metallic layer (typically 50 nm of aluminum) on a solid substrate (*e.g.* silica glass). Subsequently ultrathin polymer films are spincoated from dilute solutions directly onto the thermally evaporated metal. The top electrode is produced only at a later stage, when the upper surface of the film is capped with a second layer of metal, evaporated in the same conditions as the lower electrode. Aluminum is preferred to other metals because of the sharpness of the interfaces between this element and several polymers [49]. Evaporated on top of a polymer film, gold, on the contrary, tend to diffuse through the organic medium.

A disadvantage of nanocapacitors comes from the non-zero value of the resistance of the evaporated electrode, since the surface of thermally evaporated Al is immediately covered by a 2–3 nm layer of oxide. In terms of an equivalent electric circuit, the series of this resistance and the capacitance of the polymer layer gives rise to a peak in the imaginary part of the dielectric function [50]. The maximum of the peak corresponds to  $(2\pi RC)^{-1}$ , where  $R$  is the resistance and  $C$  is the capacitance of the film, which scales as  $h^{-1}$ ; consequently, upon reduction of the thickness, the peak shifts towards lower frequencies, limiting the investigation of relaxation spectra in the high-frequency region. Furthermore, the roughness of the metallic surface limits the investigation of extremely thin films ( $h < 3$  nm), due to the high probability of electric shortcuts.

### 1.2.2 Spaced nanocapacitors (supported films)

In order to investigate ultrathin films with a free upper surface, Serghei and Kremer proposed to employ aqueous colloidal suspension of silica particles fixing the spacing between metallic electrodes down to the length scale of 1  $\mu\text{m}$  [51]. Further development of the technique permitted to push this distance down to  $\sim 100$  nm, via the use of nanospacers, prepared by nanolithography [52].

To reduce the  $RC$  peak at high frequency, the electrodes used in this cell are fabricated using ultraflat silicon wafers with resistivity smaller than 5 m $\Omega$ . The films under investigation are spincoated on the bottom electrode, while a small amount of monodisperse silica colloids is dispersed on the bottom electrode; subsequently, the two electrodes are brought in contact and slightly pressed against each other. Alternatively, in the case of nanopatterned spacers, the polymer is spincoated on the flat electrode. Serghei and coworkers used this configuration to probe films having thickness range between 2 nm and 1  $\mu\text{m}$ . A disadvantage of this method is related to the non-linear effects in the dielectric function introduced by the presence of the airgap between the electrodes. However, neglecting the dispersive contribution of the air gap, the real and imaginary part of the dielectric permittivity

of the film can be expressed as a function of the ratio of the film thickness over the thickness of spacers,  $x$

$$\varepsilon_F'' = \varepsilon_M'' x \frac{(\varepsilon_M')^2 + (\varepsilon_M'')^2}{[\varepsilon_M' - (1-x)[(\varepsilon_M')^2 + (\varepsilon_M'')^2]]^2 + (\varepsilon_M'')^2}, \quad (8)$$

$$\varepsilon_F' = (\varepsilon_M')^2 + (\varepsilon_M'')^2 x \times \frac{\varepsilon_M' - (1-x)[(\varepsilon_M')^2 + (\varepsilon_M'')^2]}{[\varepsilon_M' - (1-x)[(\varepsilon_M')^2 + (\varepsilon_M'')^2]]^2 + (\varepsilon_M'')^2}, \quad (9)$$

where  $\varepsilon_M$  is the dielectric permittivity of the whole sample (film + air gap), while  $\varepsilon_F$  is the permittivity of the film alone.

### 1.2.3 Interdigitated comb electrodes (supported and freely standing films)

An alternative approach to measure the dielectric function of ultrathin films with one free surface is given by sensors containing interdigitated electrodes or IDEs [53–57]. The IDE sensors are composed of a metallic structure (usually gold or aluminum), laying on a substrate with extremely low dielectric permittivity  $\varepsilon_{\text{sub}}$  (quartz or fused silica). The probed films can be placed either on top of the substrate (supported) IDEs or suspended in between the fingers (freely standing).

The repeated couple of fingers can be considered as electrodes in a parallel configuration, so that the total capacitance of the sensor  $C_{\text{TOT}}$  increases proportionally with the number of fingers. Due to the presence of fringe lines, the validity of this simple linear relationship is limited to films of thickness much smaller than the height of the IDEs,  $D$ . In fact, only under the condition  $h \ll D$ , the lines of the  $E$ -field penetrate into dielectric medium, parallel to the substrate.

The spacing between the fingers  $s$  is typically in the order of a few micrometers, which makes it necessary to fabricate IDEs by means of UV lithography. The reduction of the lateral dimensions of the IDE structure to this extent permits to achieve enough sensitivity to probe ultrathin films. In fact, these sensors allow the employment of higher voltages compared to the parallel plate geometry (where the spacing is nanometric) ensuring a better signal/noise ratio, without risking non-linear effects typically encountered above 10<sup>6</sup> V/m. Following simple geometrical considerations,  $C_{\text{TOT}}$  increases upon reduction of  $s$ , as it follows from

$$C_{\text{TOT}} = \frac{C_0}{2}(1 + \varepsilon_{\text{substrate}}), \quad (10)$$

where  $C_0$  is the capacitance of the empty sensor, excluding the fringe field contribution, and it is given by [58]

$$C_0 = Npq \frac{4}{\pi a} \varepsilon_0 \sum_{n=1}^{\infty} \frac{1}{2n-1} J_0^2 \left[ \frac{(2n-1)\pi s}{2a} \right], \quad (11)$$

$J_0$  denotes the zeroth Bessel function of the first kind of the variables  $s$  and  $a = s + w$ , where  $s$  and  $w$  are, respectively, the width of the fingers and the spacing between

them.  $p$  and  $q$  are, respectively, the length of the fingers and the lateral dimension of the whole IDE (see fig. 1c).

Because of the orientation of the field, the contributions of all the sublayers (of thickness  $h_i$ ) to the total capacitance also add up according to  $C_{\text{TOT}}(\omega, T, h) = \sum C_i(\omega, T, h_i)$ . Under these conditions, the different contributions to the relaxation spectra are linearly superimposed, which permits a more straightforward discrimination among them with respect to the parallel plate configuration [59]. In view of the aforementioned advantages, IDEs present a few complications, like the presence of a non-metallic substrate, which senses the fringe lines of the electric field. Furthermore, in the case of low-molecular-weight molecules, the open configuration might allow desorption during measurements at relatively high temperatures. Nevertheless, at the state of the art, this is the only sensor permitting to investigate the dielectric function of a freely standing film both in air and in a controlled atmosphere.

#### 1.2.4 Local dielectric spectroscopy (supported films and surface processes)

The last approach described in this section is the local dielectric spectroscopy (LDS), which can be considered a special case of electric force microscopy (EFM) [60,61]. This method employs the tip of an atomic force microscope (AFM) to probe the dielectric properties of the sample [62]. A modulated voltage  $V(t) = V_0 \cos(\omega t)$  is applied to a conductive tip, which is kept a few nanometres apart from the sample surface, resulting in the polarization of the region of the sample close to the electrically charged probe. The system tip + sample has an electric capacitance, dependent on their mutual distance  $z$  and on the geometry of the tip, that in the case of thin films can be approximated as

$$C(z) = 2\pi\epsilon_0 R \ln \left\{ 1 + \frac{R(1 - \sin(\theta))}{z + h/\epsilon} \right\}, \quad (12)$$

where  $h$  is the thickness of the sample and  $\epsilon$  is its dielectric permittivity,  $\epsilon_0$  is the permittivity of vacuum,  $R$  is the radius of the tip of the probe, and  $\theta$  is a parameter describing the aperture of the whole probe tip, assumed of conical shape (see fig. 1). On the other hand, the electrostatic force between the tip and the sample induces a variation of the resonant frequency of the cantilever,  $\Delta f(t)$ , which results from the sum of three terms: a  $dc$  shift, a term at the same frequency of the modulation,  $\Delta f_\omega(t)$ , and a term  $\Delta f_{2\omega}(t) = A \cdot \cos(2\omega t - \delta)$ , where  $\delta$  is a phase lag, giving rise to the dispersive component of the capacitance.

The frequency shift can be measured by comparing the response of the cantilever before and after the excitation voltage is applied to the tip. This is achieved with a double-pass technique, which is performed in two steps: during the first pass, the sample is approached with the usual tapping-mode operation. During the second pass, the tip is lifted by a constant height, and at the same time, the voltage is applied, inducing polarization in the sample.

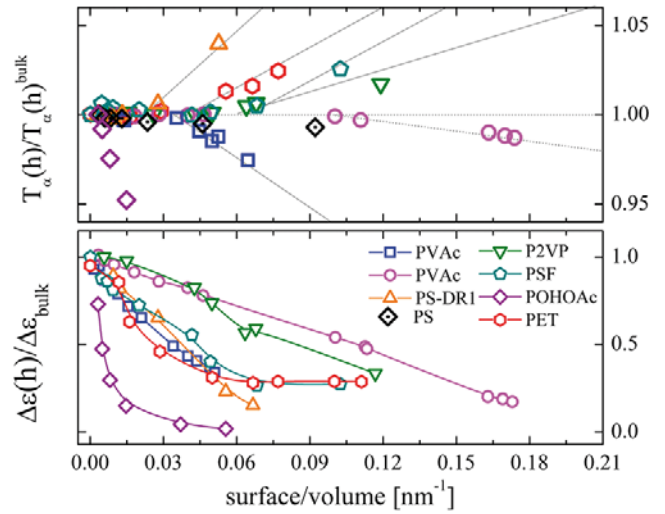


**Fig. 2.** Normalized variation of  $T_\alpha$ , at the indicated frequency, or  $T_g$  ( $\equiv T_\alpha$  at 1.6 mHz) (top panel) and  $\Delta\epsilon$ , at the indicated temperature, (bottom panel) *vs.* the surface/volume ratio (inverse of thickness) for poly(vinylacetate), PVAc (squares) ( $T_\alpha$  (100 Hz),  $\Delta\epsilon$  (333 K)); PVAc (circles) ( $T_\alpha$  (38 Hz),  $\Delta\epsilon$  (322 K)); labeled polystyrene, PSDR1 ( $T_g$ ,  $\Delta\epsilon$  (421 K)); poly(2-vinylpyridine), P2VP ( $T_g$ ,  $\Delta\epsilon$  (403 K)); polysulfone, PSF ( $T_g$ ,  $\Delta\epsilon$  (485 K)); hyperbranched polyester, POHOAc ( $T_\alpha$  (0.3 Hz),  $\Delta\epsilon$  (500 K)); poly(ethylene terephthalate), PET ( $T_g$ ,  $\Delta\epsilon$  (363 K)). Reproduced from Rotella *et al.* [65] with permission of the Royal Chemical Society.

The variation of  $\Delta f_{2\omega}(t)$  can be detected in both amplitude and phase shift,  $\delta$ , interfacing the AFM to a lock-in amplifier. A treatment of the mathematical model which allows obtaining the real and imaginary part of  $C(\omega)$  is behind the aim of this section, but it is thoroughly reported in the literature [60,61,63].

Thanks to the use of an atomic force microscope, LSD has the unique feature, among dielectric techniques, to allow probing a small portion of the film. Furthermore the local dielectric response can be associated to the morphology of the surface, which allows assessing the occurrence of concurrent processes like dewetting, during dielectric measurements. At the state of the art, such a method permits to access a broad frequency range (0.5 Hz–5 kHz) [64].

## 2 The segmental motion under confinement

### 2.1 The mean relaxation time

In fig. 2, we reported the thickness dependence of the parameters related to the segmental dynamics of a larger number of polymers investigated in the capped geometry [65]. In particular in the top panel, we plotted the values of the mean value of the structural relaxation time,  $\tau$ , proportional to the inverse of the frequency of the maximum of the relaxation peak in isothermal conditions, or of  $T_\alpha$ , the temperature of the maximum of the relaxation peak in isochronal conditions. The latter parameter corresponds to  $T_g$  if the frequency of reference is 1.6 mHz,

$(2\pi 100\text{ s})^{-1}$ . To permit a straightforward analysis, both quantities are given as a function of the inverse of the film thickness, which, in the geometry of thin films, corresponds to the surface/volume ratio. For all the systems investigated,  $\tau$  is not affected by confinement down to a thickness on the order of 20 nm (with exception of the hyperbranched polyester POHOAc where the dynamics is already perturbed at hundreds of nanometers). Below this threshold, the dynamics gets accelerated or retarded, that is,  $T_g$  decreases or increases. The molecular origins of these perturbations in the dynamics are not yet clear.

Tanaka and co-workers demonstrated that, same as for cooling, the slower dynamics in proximity of a solid interface is due to an enrichment of the isotropic liquid in “glassy structural order” (GSO) [39]. GSO here indicates the effect of many-body interactions providing bond orientational order (BOO)—*e.g.* face-centric cubic, or hexagonal close-packing in a 3D melt. The BOO, however, also favors the presence of clusters that, not belonging to any crystallographic symmetry group, are not able to tile the entire space. Although direct measurements of the BOO are not possible by conventional scattering methods, we have recently introduced an experimental approach capable to detect a variation in BOO, based on the correlation between dipole moments [57]. At the moment, the two-order-parameter (TOP) model can explain only the occurrence of slower interfacial dynamics, and cannot thus explain the reduction in  $T_g$  observed in proximity of solid interfaces, as in capped films.

Scheidler *et al.* explained the changes in the relaxation rate of molecules in proximity of an interface in terms of the roughness of the substrate [66,67]. Simulations of the structural dynamics of a Lennard-Jones liquid confined in a box with hard walls, revealed shorter relaxation times near flat walls (“zero” roughness), and increase in  $\tau$  at larger roughness. Consequently, the perturbation in the relaxation time is explained in terms of a local topological affinity between the molecules of the liquid and those of the substrate, increasing upon cooling. The memory of such a correlation fades after several molecular layers, independently of the substrate roughness. The experimental validity of these ideas is limited by the fact that a change in roughness cannot be easily disentangled from a correlated variation in interfacial energy, a quantity that strongly affects the structural dynamics. Moreover, the trends in fig. 2 disprove this criterion, in fact the data were obtained from capped films where  $T_g$  increased or decreased independently of the constant roughness of the substrate (Al layers evaporated in similar conditions).

In this regard, Fryer *et al.* [68] identified a correlation between the sign of  $\Delta T_g (= T_g^{\text{film}} - T_g^{\text{BULK}})$  and the substrate/polymer interactions, where small interfacial energies,  $\gamma_{\text{PS}}$ , correspond to reductions in  $T_g$ , while positive values of  $\Delta T_g$  should be accompanied by larger interfacial interactions, that is, values of  $\gamma_{\text{PS}}$  exceeding a critical threshold of  $2\text{ mJ m}^{-2}$ . The value of  $|\Delta T_g|$  increases upon reduction of the thickness, due to the larger weight of interfacial layers. The advantage of this criterion is that  $\gamma_{\text{PS}}$  can be promptly estimated via the Fowkes-van

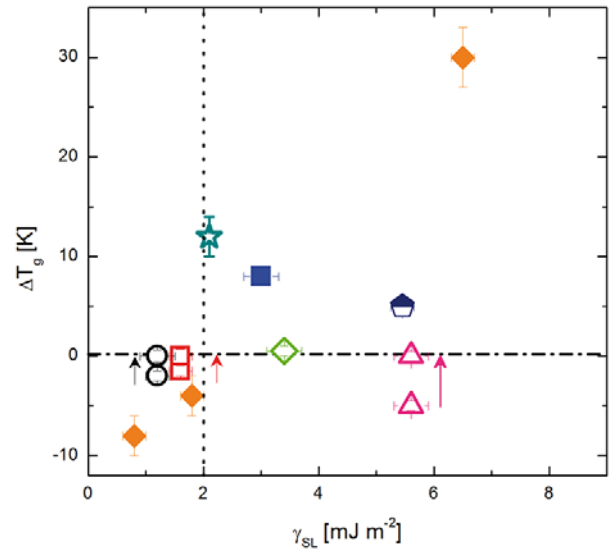


**Fig. 3.** Shift in  $T_g$  upon confinement as a function of the polymer/substrate interactions for different systems: PS/OTS (orange diamonds, 22 nm supported, [68]); PS/Al (pink triangles, 20 nm capped, [23]); poly (vinyl acetate), PVAc/SiO<sub>2</sub> (green open diamond, 22 nm, supported, [32]); PVAc/Al (red open squares, 22 nm, supported, [32]); PVAc/Au (black open circles, 22 nm, supported, [32]); poly (ethylene terephthalate), PET/Al (blue squares, 13 nm, capped, [16]); polysulphone, PSF/Al (blue pentagon, 10 nm, capped, [70]); polycarbonate, PC/Al (dark cyan star, 22 nm, capped, [71]). The arrows indicate the evolution of  $T_g$  during prolonged annealing in the liquid state.

Oss-Chaudhury-Good model of surface tension [69], starting from literature values, or via measurements of contact angles formed by (at least) three test liquids on the polymer surface and/or on the substrate [16,70,71].

Although able to describe the shift in  $T_g$  for films of PS and PMMA spincoated on octadecyltrichlorosilane (OTS), this criterion is far from being universally valid, and cannot explain the shift in  $T_g$  measured after prolonged annealing in the liquid state, see fig. 3. If we limit our attention to the intuitive arguments of finite-size and interfacial effects, then film thickness, and surface interactions should be sufficient to univocally determine the deviations from bulk behavior, that is, given a pair polymer/substrate, the  $T_g$  of a film of fixed thickness should be unique. On the contrary, we demonstrated that it is possible to tune the  $T_g$  of a film without altering the quality of the spincoating solvent (same entanglement density), or the nature of the substrate (same interfacial interactions) or the film thickness (constant surface/volume ratio) [18,23].

In the following subsections, we describe our experimental evidence correlating the deviation from bulk dynamics to the content of free volume in the layer irreversibly adsorbed at the polymer/substrate interface. First, we identify the signatures of irreversible chain adsorption on the structural dynamics; then, we describe how adsorption can induce both reductions and increases in the glass transition temperature; finally, we provide

a correlation between  $\Delta T_g$  and the interfacial free volume, revealing the contribution of packing frustration on the enhancement of the structural dynamics.

## 2.2 The dielectric strength

In the bottom panel of fig. 1, we plotted the thickness dependence of the intensity of the structural peak,  $\Delta\varepsilon$ . Upon increase of the surface/volume ratio, the dielectric strength decreases, regardless of whether thinner films exhibit a higher or lower  $T_g$ .  $\Delta\varepsilon$  is the contribution of orientational polarization to the dielectric constant [41], which in isothermal conditions is proportional to  $g \cdot \langle \mu^2 \rangle$ , where  $\langle \mu^2 \rangle$  is the mean square dipole moment, and  $g$  is the Kirkwood correlation factor, taking into account the orientational correlation among dipole moments,  $g = 1$  in case of random orientation, and it increases when dipoles are oriented more parallel to each others. Approximating the previous expression at constant  $g$ ,  $\Delta\varepsilon \sim \tilde{N} \mu^2$ , where  $\tilde{N}$  indicates the density number of dipole moments, allows assigning a perturbation in the dielectric strength to a change in the number of segments relaxing on the time scale of  $\tau$ . The drop in  $\Delta\varepsilon$  observed upon confinement hints at a reduction of the molecules contributing to the orientational polarization. Remarkably, a similar phenomenon was observed upon prolonged annealing in the liquid state. Measurements of the dielectric function of ultrathin films of PS performed in isothermal conditions at  $T > T_g$ , revealed an extremely slow reduction of the dielectric strength upon thermal annealing [23]. This drop in  $\Delta\varepsilon$  cannot be rationalized in terms of release of mechanical stresses, because it takes place on time scales much longer than the structural and the terminal relaxation (reptation) time,  $\tau_{\text{REP}}$ . The reptation model predicts that full equilibration of the film is reached at time scales on the order of  $\tau_{\text{REP}}$ , after that chains have completely disentangled from the tube induced by screening of neighboring segments. Similar trends were reported for PMMA [24], PVAc [64], PS labeled with polar moieties [72] and PET [73] (for this semicrystalline polymer we carefully checked that crystallization was not involved). Also in this case the reduction in  $\Delta\varepsilon$  hints at a reduction in  $\tilde{N}$ , that is, chain immobilization and the consecutive inhibition of fluctuation of dipole moments over large solid angles.

Experiments performed in a multilayer geometry, where we selectively placed chains of PS labeled with the polar dye dispersed red 1 (DR1) (see subsect. 4.4), permitted to verify that the reduction in orientational polarization is active only when the chains are in contact with a solid interface [11]. In fact, layers of PS-DR1 capped between films of neat PS did show a bulk-like  $\Delta\varepsilon$ , while layers of the doped polymer spincoated on aluminum showed a significant drop in dielectric strength, increasing upon thermal annealing. An identical behavior was observed in the case of films of PS-DR1 onto which we had previously evaporated Al. This evidence, combined with calorimetric scans of bulk samples, permitted to discard the presence of crystallization and crosslinking (other two possible sources of chain immobilization), and we speculated that

the reduction of  $\Delta\varepsilon$  is due to the irreversible adsorption of monomers onto the substrate (*hypothesis 1*). Consequently, the deviation from bulk behavior would originate from the peculiar non-equilibrium conformations assumed by the absorbed chains at the polymer/solid interface (*hypothesis 2*).

## 2.3 Correlating adsorption to perturbations in the orientational polarization

*Hypothesis 1* implies that the drop of  $\Delta\varepsilon$  upon annealing follows the kinetics of irreversible chain adsorption. In other words, the decay rate of the dielectric strength should be sensitive to the different regimes that characterize the adsorption of monomers onto the substrate. Considering the complexity in the reorganization of the chains upon adsorption onto a solid substrate, we expected to have different mechanisms yielding a drop of  $\Delta\varepsilon$ , *e.g.* local changes aiming at increasing the number of polymer-substrate contacts/surface and incorporation of new chains into the adsorbed layer. To test these ideas, we designed a series of experiments which enabled to monitor  $\Delta\varepsilon(t)$  and kinetics of thickening of the polymer layer irreversibly adsorbed from the melt onto the substrate,  $h_{\text{ads}}(t)$ , during isothermal annealing in the liquid state [23]. While the former quantity was measured continuously, the latter one was determined independently at different annealing times,  $t_{\text{ANN}}$ , (corresponding to different samples) in the same experimental conditions.

To avoid the impact of mechanical stresses due to spincoating, we worked with films previously “equilibrated” during a pre-annealing step much longer than  $\tau_{\text{REP}}$ . Noticing that the linear deconvolution of the electrical impedance of the whole film, as the sum of the capacitance of the sublayers, is ensured only for non-polar systems (*i.e.* where  $\Delta\varepsilon/\varepsilon_\infty \ll 1$ ) [59], we have chosen polystyrene ( $\Delta\varepsilon/\varepsilon_\infty \approx 0.016$ ), as model system. Nevertheless, PS has a dielectric strength large enough to be determined precisely by an impedance analyzer, and its adsorption kinetics is slow enough to permit monitoring the process in real time.

We annealed a 21 nm thick film of PS97 (where 97 is the weight average molecular weight,  $M_w$  expressed in kg/mol) at  $T_g^{\text{BULK}} + 50$  K (423 K), prepared as a nanocapacitor (Al/PS/Al). Exploiting the symmetric character of this confinement geometry (see subsect. 1.2.1), we reduced the number of free parameters and could concentrate on the adsorbing interface, without feeling the effects of a surface in contact with air or vacuum. After an annealing time,  $t_{\text{ANN}} \sim 27$  h (consider that  $\tau \sim 10 \mu\text{s}$  and  $\tau_{\text{REP}} < 1$  s),  $\Delta\varepsilon$  decreased by almost 30%, while the electric capacitance in the absence of polarization contributions,  $C_\infty$ , increased by  $\sim 3\%$ , see fig. 4. Due to the direct proportionality between capacitance and the inverse of the thickness of the dielectric medium, the higher value of  $C_\infty$  indicated a negligible shrinkage of the film ( $\sim 1 \text{ \AA}$ ). On a logarithmic scale, we noticed a constant reduction rate of  $\Delta\varepsilon(t)$  till  $t_{\text{ANN}} \sim 2 \cdot 10^3$  s; after this induction time and

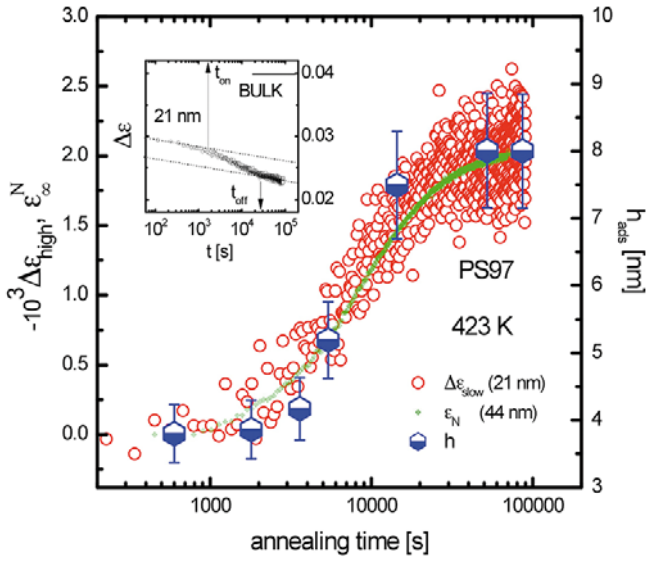


**Fig. 4.** Comparison between the time evolution of the component of the dielectric strength with higher decaying rate,  $\Delta\epsilon_{\text{high}}$ , (for a 21 nm thick film of PS97), the dielectric constant (44 nm, PS97) and the thickness of the irreversibly adsorbed layer obtained in the same annealing conditions (423 K). To ease comparison, we normalized the dielectric constant between the starting and final value of  $\Delta\epsilon_{\text{high}}$ . In the inset: time evolution of the dielectric strength (21 nm), the dash-dotted lines indicate the traces of  $\Delta\epsilon_{\text{low}}$ , *i.e.* the logarithmic decay of  $\Delta\epsilon$  at short and long annealing times. Reproduced from Napolitano *et al.* [23] with permission of the Nature Publishing Group.

up to  $t_{\text{ANN}} \sim 3 \cdot 10^4$  s (see fig. 4), the decay increases by a factor 0.6.

For films of different thicknesses, we observed similar trends although to different extents. In particular, thicker films had relatively smaller reduction in  $\Delta\epsilon$ , in line with the idea that we are dealing with an interfacial phenomenon. We explained the appearance of the discontinuities in  $\Delta\epsilon$  as the superposition of two processes characterized by different rates, designated as “low” and “high”, appearing respectively as a logarithmic contribution (linear background in a representation of  $\Delta\epsilon$  *vs.*  $\log(t)$ ) and an exponential decay of characteristic time scale  $t_{\text{high}}$ .

$$\frac{\Delta\epsilon(t)}{\Delta\epsilon(0)} = 1 - \Lambda \log(t/t_0) - \Sigma [1 - \exp(-t/t_{\text{high}})], \quad (13)$$

where  $t_0$  is a sufficiently short time that we fixed to 1 s, and  $\Lambda$  and  $\Sigma$  are, respectively, the low and the high decay rate of the drop in dielectric strength.

The thickness of the irreversibly adsorbed layer was obtained via Guiselin’s experiment [74], where the non-adsorbed chains are separated from the layer irreversibly adsorbed onto the substrate upon washing in the same good solvent used for spincoating. Investigations of melts of PMMA [75] and PS [18] proved that the thickness of irreversibly adsorbed layer (at constant  $t^* = t_{\text{ANN}}/t_{\text{ads}}$ , see subsect. 2.4) scales with  $N^{1/2}$ , where  $N$  is the polymerization degree. This scaling is in line with a reflected

random walk and validated the idea of Guiselin that interfacial conformations are preserved within this procedure. The thickness of the Guiselin brushes,  $h_{\text{ads}}$ , increased with a saturating exponential,  $h_{\text{ads}}(t) \sim 1 - \exp(-t/t_{\text{ads}})$ . When plotted as a function of the logarithm of the annealing time,  $h_{\text{ads}}(t)$  shows discontinuities in correspondence of those in  $\Delta\epsilon(t)$ , and an impressive affinity with  $\Delta\epsilon_{\text{high}}(t)$ . The same results were reproduced in further experiments performed in different conditions, where we varied the annealing temperature, the molecular weight, and the monomer. Consequently, we assigned  $\Delta\epsilon_{\text{high}}(t)$  to the process of growth of the irreversible adsorbed layer, proceeding via addition of new chains. Chain pinning brings to a partial or total immobilization of monomers at the interface, which hinders the structural relaxation, via a severe reduction of the solid angle over which dipoles can reorient. This limitation yields an effective lower mean square dipole moment and thus a lower  $\bar{N}$ . The direct proportionality between the thickness of Guiselin brush and the drop in dielectric strength,  $|\delta\Delta\epsilon_{\text{high}}| \sim \delta h_{\text{ads}}$ , implies that the adsorbed layer is built up in a progressive fashion, where each immobilized chain contributes in the same way to the thickening. This conjecture was finally verified, see subsect. 2.5.2, by proving that  $\delta h_{\text{ads}} \sim \delta\sigma$ , where  $\sigma$  is the surface coverage.

## 2.4 Kinetics of irreversible chain adsorption and the dimensionless number $t^*$

Based on the trend generally observed in dilute solutions, we propose a time evolution of the thickness of the layer irreversibly adsorbed from polymer melts, including a crossover between a power law and a logarithmic growth,

$$h_{\text{ads}}(t) = \begin{cases} h_{t=0} + vt^\alpha, & t < t_{\text{cross}}, \\ h_{t_{\text{cross}}} + \Pi \log t, & t > t_{\text{cross}}, \end{cases} \quad (14)$$

where  $t_{\text{cross}}$  is the crossover time,  $v$  and  $\Pi$  express the growth rates in the different regimes and  $\alpha$  indicates the type of diffusion processes involved. The slower growth rate at  $t > t_{\text{cross}}$  is due to a change in the chain conformations in the adsorbed layer. The first chains arriving on the substrate ( $t < t_{\text{cross}}$ ) spread onto the surface and adopt flat conformations, where the component of the gyration radius parallel to the substrate exceeds the perpendicular one. At larger values of  $\sigma$ , the probability to find sufficiently large spots permitting flat conformation decreases and insertion of new chains is possible only via relaxation of previously adsorbed chains [76,77]. Moreover, as the number of polymer/substrate contacts per chain drops upon annealing, at  $t > t_{\text{cross}}$ , before adsorbing molecules have to stretch to diffuse through the existing layer. In this second regime, the number of trains (adsorption of consecutive monomers) is reduced, while that of loops increases [78]. Although adsorption yields a reduction in free energy due to the enthalpic gain achieved upon pinning, the reduction in the number of allowed conformations in this late stage of adsorption corresponds to a severe entropy loss. On this regard, Ligoure and Leibler [79]

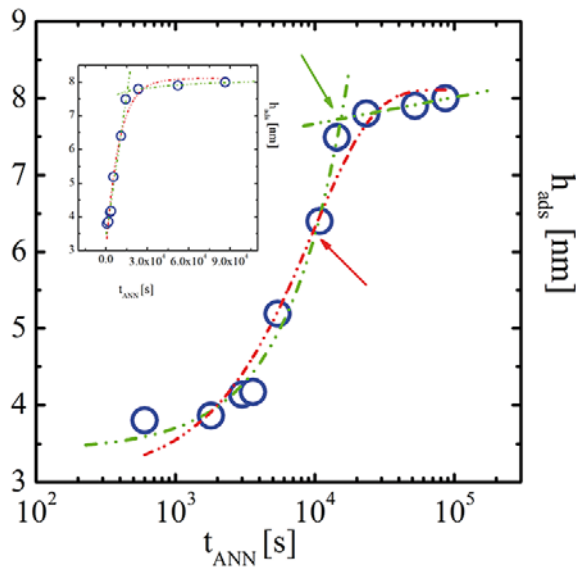


**Fig. 5.** Comparison between an exponential fit (red line) and a power law/logarithmic fit (green line) for the kinetics of thickening of the layer irreversibly adsorbed from melts of PS97 onto Al, at 423 K. The red arrow indicates the characteristic adsorption time,  $t_{\text{ads}}$ , while the crossover time,  $t_{\text{cross}}$ , is indicated in green. The same data are plotted in the inset as a function of the time of annealing in a linear scale.

recognized that previously adsorbed chains can be considered as a potential opposing to thickening of the interfacial layer. The resulting reduction in the growth rate is well described by a logarithmic regime, confirmed by simulations and successive experiments. With these considerations in mind, we introduced a dimensionless number  $t^* = t_{\text{ANN}}/t_{\text{cross}}$ , which is particularly helpful in the description of the changes in the adsorbed layer upon the transition in the structure of the adsorbed layer during its formation [23].  $t^*$  was furthermore used to define a criterion for equilibration of polymer melts near an interface [80] and to determine the onset of the regime of confinement where the crystallization rate significantly deviates from bulk value in semicrystalline polymers [73].

Due to the large errors in the determination of  $h_{\text{ads}}$  (or of the adsorbed amount), however, several authors preferred to describe the kinetics of thickening of the Guiselin brush via a more general exponential form of the type [75]

$$h_{\text{ads}}(t) = h(t=0) + h_{\text{ads}}^{\text{max}} \{1 - \exp[-(t/t_{\text{ads}})^\beta]\}, \quad (15)$$

where  $h_{\text{ads}}^{\text{max}}$  is the thickness of the layer after long annealing time ( $t^* \gg 1$ ) and  $t_{\text{ads}}$  a characteristic time always smaller than  $t_{\text{cross}}$ , in the particular case of PS97 on Al  $t_{\text{cross}}/t_{\text{ads}} \approx 1.4$ , see fig. 5. We stress that  $t^*$  should not be interpreted as an absolute value, but just as an order of magnitude, consequently, as  $t_{\text{cross}} \sim t_{\text{ads}}$ , we can alternatively define  $t^* = t_{\text{ANN}}/t_{\text{ads}}$ .

In the case that the slope of the logarithmic growth is not too large, it is not possible to distinguish between the “power law/logarithmic” and the “saturating exponential” scenario, especially when the data are plotted as a

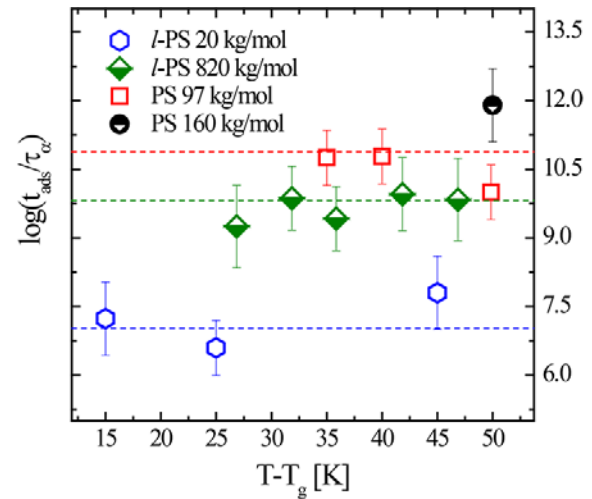


**Fig. 6.** Ratio between the characteristic adsorption time,  $t_{\text{ads}}$ , and the structural relaxation time,  $\tau$ , for several polymers.

function of the time, and not of its logarithm, see fig. 5. In addition to having less free parameters (4 vs. 6), although less precise, the exponential fit permits to estimate a characteristic time also in the case that the crossover to the logarithmic regime is not experimentally observable (as in the case of extremely slow processes, or fast degradation). The meaning of the exponent  $\alpha$  is more evident if we approximate eq. (15) at short annealing times, for  $t \ll t_{\text{ads}}$  we have  $h_{\text{ads}}(t) \sim t^\beta$ , thus  $\alpha = \beta$ . If we assume that in the early stages of adsorption the surface coverage is limited by Brownian motion along the direction  $x$ ,  $\langle x^2 \rangle \sim \sigma \sim t$ , and considering that  $\delta\sigma \sim \delta h_{\text{ads}}$  see subsect. 2.5.2, then we get  $h_{\text{ads}}(t) \sim t$  and  $\beta = 1$ , a trend observed for melts of PS [23], PMMA [75] and PET [73].

The low rate drop in  $\Delta\varepsilon$  is due to reorganizations in the adsorbed layer, aiming at minimizing free energy, via an increase of contact/surface ratio, without incorporation of new chains. This process has an analogous dielectric signature as crystal perfectioning during secondary crystallization [81], and starts before reaching the measurement temperature. This observation is in line with the non-zero value of  $h_{\text{ads}}$  at short annealing times, or similarly to values of  $\Delta\varepsilon(t_{\text{ANN}} = 0)$  smaller than in bulk, and implies that adsorption takes place already in solution during spincoating.

Our investigation of adsorption via dielectric spectroscopy continued by analyzing the temperature dependence of the adsorption time in a series of samples of PS of different  $M_w$ , both homopolymers and partially decorated with polar moieties spincoated on Al [72]. The value of  $t_{\text{ads}}$  drastically increased upon cooling, in line with the idea that adsorption is mostly governed by diffusion. As the temperature dependence of the diffusion of a chain in its own melt was not known for all the systems investigated, to further check the validity of this scaling, we compared  $t_{\text{ads}}(T)$  to  $\tau(T)$ , which can be deduced in the same annealing experiment. The temperature dependence of the structural time (rotational motion) is in fact similar, although not identical, to that of translation modes [82].

For all the systems investigated, the order of magnitude of the ratio  $t_{\text{ads}}/\tau$  seems temperature independent, implying that the activation energy of irreversible chain adsorption is comparable to that of the structural relaxation (see fig. 6). Such a strong coupling permits to estimate the value of  $t_{\text{ads}}$  also in the case of prohibitive experimental conditions. In fact, while  $\tau(T)$  can be easily measured also below the calorimetric  $T_g$ , the transition between the power law and the logarithmic regime can be experimentally detected only at much higher temperatures, *e.g.* for PS97  $\log(t_{\text{ads}}/\tau)$  is 10.5, that is, at  $T_g$  where  $t = 100\text{--}1000\text{ s}$ ,  $t_{\text{ads}} \approx 10^{13}\text{ s} > 30000$  years.

## 2.5 Correlation between interfacial structure and global film dynamics

### 2.5.1 Glass transition temperature and the thickness of the irreversibly adsorbed layer

To validate our hypothesis on the correlation between conformations in the adsorbed layer and dynamics (*hypothesis 2*), we formalized the link between the structure of the adsorbed layer and the segmental motion. We assumed that the shift in the glass transition temperature of a thin polymer film is enslaved to the  $T_g$  of the layer irreversibly adsorbed onto the substrate and that the structural dynamics is governed by the local abundance of free volume [18]. Considering that the adsorbed layer is formed by gradual filling of empty sites present at the polymer/substrate interface, we speculated that in the early stages of adsorption ( $t^* < 1$ ), the content in free volume exceeds the bulk value. This excess in free volume can be treated as packing frustration inducing an enrichment in the population of segments relaxing with faster dynamics, that is, a reduction in  $T_g$ . Upon further annealing, more chains adsorb at the interface, and the excess in free volume drops, yielding an increase in  $T_g$ , with respect to the value at shorter annealing time. At  $t^* \gg 1$ , two scenarios are possible:

- 1) the adsorbed layer has a free volume content as in bulk, then  $\Delta T_g = 0$ ,
- 2) the adsorbed layer is denser than much thicker films, then  $\Delta T_g > 0$ .

We could verify the proportionality between the interfacial free volume and  $\Delta T_g$  [18], but it is still not clear why, after annealing at times much longer than the crossover time, the  $T_g$  of some in systems tends towards the bulk value (no deviation from bulk value) and why in some others an increase in  $T_g$  is instead finally observed.

Focusing on the impact of polymer/solid interfaces, we concentrated on capped film, where no free surface is present. This permitted to deal with symmetric profiles of molecular mobility, see subsect. 4.4, and proceed to a straightforward analysis of our results. To verify our conjecture on the link between  $T_g$  and  $h_{\text{ads}}$ , we measured, by means of capacitive dilatometry [15,83], the  $T_g$ 's of films of PS (thickness 20 nm) of different  $M_w$  after different annealing times at 423 K. To avoid changes in the adsorbed content, the cooling scan used to determined  $T_g$

started at 413 K, where the adsorption kinetics is intrinsically slower. As expected, the shift in  $T_g$  followed the same kinetics as the irreversible adsorption process [23], thus  $T_g(t) \sim h_{\text{ads}}(t) \sim \Delta\varepsilon(t)$ , which is in line with the correlation found by Srivastava and Basu [84] between the shift in  $T_g$  in nanocomposites and the thickness of the polymer/filler interfacial layer. For PS capped between Al layers,  $T_g$  is reduced compared to the bulk value at  $t^* \ll 1$ , and  $\Delta T_g$  reaches 0 at  $t^* \gg 1$ . Consequently  $t^*$  can be seen as a Deborah number of the deviations from bulk behavior, indicating the observation time necessary to erase the reduction in  $T_g$ , due to packing frustration, which in the case of scenario 1 ( $\Delta T_g = 0$ ,  $t^* \gg 1$ ) corresponds to the recovery of bulk conditions.

### 2.5.2 Reduction in $T_g$ as an effect of packing frustration on the interfacial free volume: A molding approach

Further evidence on our physical picture connecting the interfacial free volume to the  $T_g$  of ultrathin films came from the analysis of the distribution in relaxation times,  $g(\ln \tau)$  at different  $t^*$  [23]. In the case of PS on Al, adsorption induces a pronounced cutoff of the faster relaxation modes. In fact, after moderate annealing times ( $t^* \sim 1$ ), we observed a reduction in the short times component of  $g(\ln \tau)$ . Further annealing ( $t^* > 1$ ) induces a reduction in the polymer segments relaxing at slower times, characteristic of the reduction in the concentration of trains, adsorption of consecutive monomers, in fact, increases the energetic barriers related to rotational motion. Similar trends are found in systems like poly(4-tert-butylstyrene) (PTBS) [19], a linear polymer containing a bulky side group, promoting the excess in interfacial free volume where we found a paradoxical reduction in  $T_g$  accompanied by a drop in thermal expansion, see subsect. 4.6.2. Analysis of the thermal expansion profile confirmed the presence of a region with higher thermal expansion between an immobilized layer and the bulk, where an excess in free volume, justifying the lower  $T_g$ , should be located. Further indirect proofs of the role of interfacial free volume come from the observation that well annealed films of PVAc exposed to controlled humidity do not uptake as much water as films annealed at shorter times [64]. The transition from a hydrophilic to a hydrophobic character was justified considering that “well-annealed” films might achieve density values larger than in bulk, and thus have less free volume for the water molecules. Moreover, manipulation of bulk samples via dry-freezing, permitted to verify that the glass transition temperature decreases upon increase of the interchain distance, which is in line with our idea [85]. Wöll and coworkers demonstrated that the heterogeneous character of the glassy dynamics is attributed to the gradient of density and free volume in supported films [86,87]. Recent simulations by Tito *et al.* [88] further strengthened this link, showing how the propagation of free-volume colonies affects the glassy dynamics. de Gennes proposed that free volume can be transported within the film via the propagation of “kinks” along loops formed on the chains [89]. Lipson and Mill-

ner further verified that this mechanism is quantitatively in line with the deviations on the  $T_g$  of thin films [33]. Glynos *et al.* proposed that the increase of  $T_g$  on high-functionality and low-arms-molecular-weight star-shaped polymers is due to the inhibition of the mechanism suggested by de Gennes [28].

Star-shaped polymers, in fact, tend to pack more efficiently than their linear analogs in proximity of the free surface. Cangialosi, Boucher and coworkers showed that the decoupling between segmental mobility and the dilatometric glass transition can be related to the diffusion of free volume holes towards the interface [34,90–94], and a similar concept was used to provide a molecular picture for physical aging [95,96]. To quantitatively verify our picture, we designed a novel experimental method, able to quantify the changes in the dynamics upon the reduction of the amount of interfacial free volume,  $\zeta$ , here intended as space available for the molecular relaxation [18].

Our assumptions imply that the increase in  $h_{\text{ads}}$  should be linearly proportional to the reduction of free volume at the polymer/metal interface

$$\zeta(t^*) \sim \text{const} - h_{\text{ads}}(t^*) \quad (16)$$

and that an increase in interfacial free volume should correspond to a reduction in  $T_g$

$$\zeta(t^*) \sim \text{const} - \Delta T_g(t^*). \quad (17)$$

The use of  $t^*$ , rather than  $t$ , indicates the possibility to rescale data sets with different adsorption kinetics.

We could not obtain values of  $\zeta$  via scattering techniques due to reduced volume and the small density difference ( $\leq 1\%$ ) of the samples; similar complications were encountered via scanning probe microscopy because of the difficulties related to the characterization of buried interfaces and thin films. Moreover, while we expect that the value of  $\zeta$  is a constant fixed by  $t^*$ , the spatial distribution of virtual holes constituting the interfacial free volume, instead, fluctuates on the time scale of  $\tau$ . To overcome these issues, we introduced a molding-like approach where the Guiselin brushes were in direct contact with a reservoir of probe molecules [18]. Upon thermal annealing the probes diffuse inside the adsorbed layer and irreversibly adsorb in the volume still free at the PS/Al interface, see fig. 7 for a cartoon of the experiment. The drop in  $\Delta\varepsilon_{\text{high}}$  of the probe after a long diffusion time provided a measurement of  $\zeta$ .

For this experiment, we built up multilayer films of a low molecular weight ( $M_w \sim 20k$ , thickness  $h_{\text{l-PS}} = 50\text{ nm}$ ) polystyrene labeled with {4-[(4-cyanophenyl) diazenyl] phenyl}(methyl)amino, a highly polar side group (l-PS) [97], on top of the irreversibly adsorbed layers of PS. The measurements were performed in the same way as for single layers of PS, that is, in the capped geometry; due to ratio between the thickness of PS and that of l-PS and the much higher dielectric strength of l-PS, the dielectric strength of the Guiselin brush was  $< 4\%$  of the total dielectric strength of the multilayer, and thus neglected in the analysis. Based on the correlation between  $\tau$  and  $t_{\text{ads}}$ ,

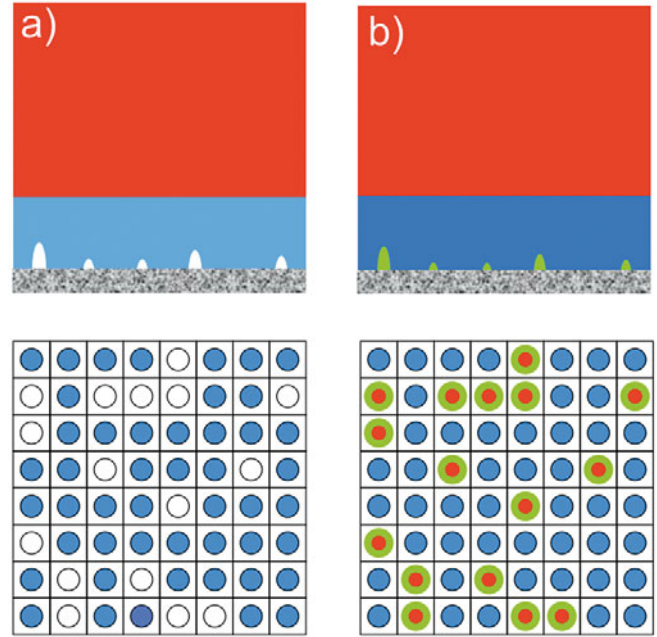


**Fig. 7.** Scheme (not to scale) of the molding approach used to determine the interfacial free volume  $\zeta$  (white circles in the left lower panel), seen here as the opposite of the surface coverage of PS (blue circles). a) To determine  $\zeta$ , we placed a thick film of l-PS (a probe oligomer, red) on top of the interfacial layer of PS (blue). b) The probes diffuse into the interfacial layer and finally occupy the free volume at the PS/Al interface, not yet occupied by PS (green). We follow the reduction of dielectric strength while the probes irreversibly adsorb (green/red circles). The final drop in  $\Delta\varepsilon$  is proportional to the number of probes immobilized, and thus to the interfacial free volume. Reproduced from Napolitano *et al.* [18] with permission of the American Chemical Society.

the samples were annealed at 398 K, a temperature where the adsorption kinetics of PS97 on Al takes place over 10 days, that is, the adsorption degree of the Guiselin brush is constant during the molding experiment.

Same as what observed for single PS layers,  $|\Delta\varepsilon_{\text{high}}(t)|$  increased after an induction time necessary for the diffusion of l-PS over the layer of PS, followed by adsorption onto Al [97]. At much longer annealing times the majority of the available space at the PS/Al interface was finally filled by l-PS segments, and  $|\Delta\varepsilon_{\text{high}}(t)|$  reached an almost constant value (a constant value is expected by approximating this quantity in the form eq. (15)). Consequently our molding-like approach allowed estimating the local free volume as

$$\zeta \equiv \lim_{t \rightarrow \infty} [\Delta\varepsilon_{\text{high}}(t)]. \quad (18)$$

This correlation is possible because the final drop in  $\Delta\varepsilon_{\text{high}}$  (obtained via an exponential approximation) is proportional to the amount of segments of l-PS that could eventually adsorb on the interfacial free volume not already occupied by chains of PS.

In line with our expectations, for interfacial layers of PS97 extracted from bulk-like samples annealed in the

condition  $t^* < 1$  (*i.e.* less for than 14 h at 453 K),  $\zeta$  followed the scaling  $\text{const} - h_{\text{ads}}$ . On the contrary, for Guiselin brushes prepared at  $t^* > 1$ , the reduction in  $\zeta$  was more pronounced, in line with the onset of a rearrangement in the structure of the adsorbed layer, favoring more efficient packing, that is, containing less specific free volume. Samples annealed for  $t_{\text{ANN}} > 14$  h resulted in  $\zeta = 0$ , in line with the recent results of Gin *et al.* [80], revealing a lack of thermal expansion in samples prepared at  $t^* \gg 1$ .

To complete the validation of eq. (17), we prepared interfacial layers having comparable thickness (within 0.5 nm), annealed for the same  $t_{\text{ANN}}$ , but different  $M_w$  and thus different  $t^*$ . Regardless of the  $M_w$ , all the new samples corresponded to  $t^* \ll 1$ , and their free volume content was comparable to that of PS97 prepared in the same conditions. The impact of the changes in interfacial free volume is not limited to the chains at the very interface. Broad experimental evidence supports the idea that the influence of substrate interactions, which we can read here as the effect of adsorption, propagate over larger length scales, proportional to the gyration radius (statistical dimension of a random coil)  $R_g$ , which can exceed hundreds of nanometers [98,99]. Although at early stages, only segments at the very interface are subjected to those conformational changes, prolonged annealing enables the formation of loops whose centre of mass is located at several tens of nm away from the polymer solid interface.

The use of samples having similar thickness but different  $t^*$  permitted also to finally verify that the thickness of the sample is not a key parameter in the deviation from bulk behavior. In fact, the determination of the glass transition temperature of samples of constant thickness ( $\sim 20$  nm), and the same molecular weight and annealing conditions as those used to determine the interfacial free volume, validated eq. (17), see fig. 8. Consequently we were able to assign the molecular origin of the enhancement in glassy dynamics in proximity of an adsorbing interface to a localized reduction in monomer density. We are currently performing further experiments to check the validity of such a correlation in the case of slower interfacial dynamics (*scenario 2*,  $\Delta T_g > 0$ ,  $t^* \gg 1$ ).

In conclusion, film thickness and interfacial interactions are not sufficient to fully predict the properties of macromolecules under confinement; models trying to describe the deviation from bulk behavior should also consider the perturbation in the free volume arising from chain adsorption.

## 2.6 Slow adsorption kinetics, re-entanglements dynamics and non-equilibrium

The correlation between the interfacial free volume and the glass transition temperature of capped thin films highlighted in the previous section implies that the deviation from bulk behavior have a finite lifetime. Consequently, the properties of polymers confined at the nanoscale level should be associated to metastable thermodynamic states [100], evolving towards equilibrium via a driving

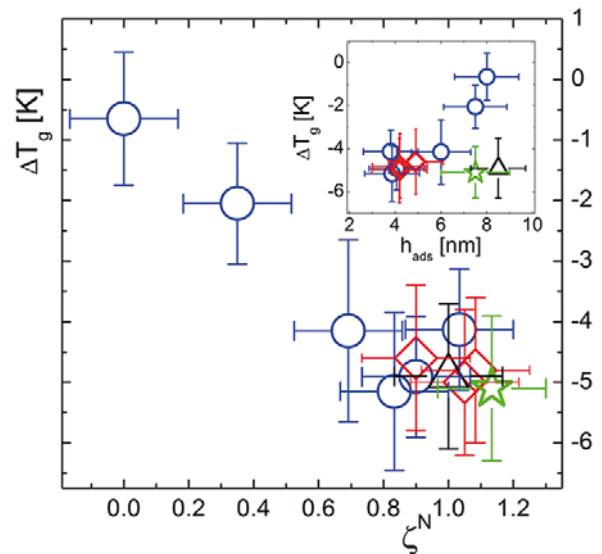


**Fig. 8.** Correlation between the local free volume and the shift in  $T_g$  for PS97 (blue circles), PS160 (red diamond), PS640 (green star), PS932 (black triangle). In the inset, shift in  $T_g$  as a function of the thickness of the irreversibly adsorbed layer. Reproduced from Napolitano *et al.* [18] with permission of the American Chemical Society.

force, which in our reasoning is arising from irreversible chain adsorption. In the next subsections we review previous literature on the “equilibration” conditions for thin films, relating it to adsorption phenomena.

The signature of non-equilibrium on the dynamics and on the static properties of thin polymer layers is marked by the presence of extremely slow relaxation processes, of a time dependence on the value of quantities measured during prolonged annealing in the liquid state, at  $t_{\text{ANN}} \gg \tau_{\text{REP}}$ . Reiter and de Gennes proposed that the metastable nature of thin polymer films is due to the formation of an internal rigid chain network, induced by the fast solvent evaporation [101]. While the network is stable upon thermal treatment in the glassy state, the authors suggested the possibility to recover equilibrium upon prolonged annealing in the liquid state, at times exceeding  $\tau_{\text{REP}}$ . Once this condition is reached, the network would heal and the film, if not thick enough, would become unstable towards long-range van der Waals interactions, causing rupture and dewetting [102]. Such a phenomenon can be avoided if the adsorption of chains in the proximity of the interface is energetically favorable. Moreover Reiter and de Gennes recognized that the formation of a Guiselin brush might strengthen the network and thus increase the lifetime of the metastable state. Recent experimental evidence seems to validate this idea, suggesting that the stability of thin films against “equilibration” actually requires time scales much longer than the reptation time. Barbero and Steiner probed the rheology of films of PS on Si by stimulating thermal fluctuations via an electric field [103]. They found that the viscosity of as-cast films is smaller than in bulk, and that prolonged annealing above  $T_g$  (equilibration time,  $t_{\text{eq}} \gg \tau_{\text{REP}}$ ) are

not always sufficient to recover the bulk condition. Further investigation confirmed the first trends and the impossibility to equilibrate high molecular weight samples [104]. Similar experiments were performed by Tsui and coworkers, who analyzed the surface viscosity via atomic force microscopy [105].

The origin of such long-lasting metastable states was imputed to the fast solvent evaporation leaving the chains in non-equilibrium conformations, where the overlap among random coils could not reach the melt limit [104,105]. At the concentrations characteristic of nanometers-thick films ( $\sim 1-10^{-2}$  w/w%), chains are organized in circumscribed random coils, not overlapping with each other. During spincoating, the solvent content drops and when the volume fraction of the polymer reaches a critical value, the film vitrifies [106,107]. The chains are thus trapped in packing geometries with a lower entanglement density, yielding a lowered viscosity.

But why do chains do not reach equilibrium when annealed for  $t > t_{\text{REP}}$ ? The ambiguity of equilibrium conditions based on reptation arises from the assumption that the time necessary to escape the virtual tube exerted by neighboring chains (disentanglement time,  $\tau_{\text{REP}}$ ) equals the time necessary to build up the entanglement network starting from two separated random coils (re-entanglement time,  $t_{\text{eq}}$ ). On the contrary, molecular dynamics simulations revealed that the re-entanglement time can exceed by several orders of magnitude  $\tau_{\text{REP}}$ , due to the low rate of successful collisions between coils permitting wetting between two single entities, followed by interpenetration [108]. Teng *et al.* reported a separation between  $t_{\text{eq}}$  and  $\tau_{\text{REP}}$  larger than 2–4 orders of magnitude, by measuring the decay in elastic modulus of freeze-dried samples of PS205 during annealing in the liquid state ( $T_g + 50$  K) [109]. Xue and coworkers had previously verified that in freeze-dried samples, the interchain distance exceeds the normal bulk values, implying a less efficient interpenetration [85].

In addition to the re-entanglement process, we need to consider also the role of irreversible chain adsorption, as a concurrent driving force keeping the system out of equilibrium over time scales much larger than  $\tau_{\text{REP}}$ . Differently than small molecules, polymers encounter larger difficulties in reaching equilibrium conformations [110]. After adsorption of a monomer onto the substrate, the rest of the chain can spread over the available surface before adsorbing on the next available pinning site. Similarly as in the case of a non-patrolled parking space, such a sluggish kinetics does not permit to cover efficiently the surface. Thus, if previously adsorbed chains cannot relax via reduction of the number of contacts per unit area, chains arriving at a later stage need to stretch and diffuse through the existing layer to further reduce the free energy [77, 111]. The logarithmic growth in the latest stage of adsorption is a signature of this phenomenon [79,112]. Further experimental evidence of this dual mechanism was provided, for example, by infrared analysis of conformational substrates [113], a combined investigation of dielectric spectroscopy and secondary harmonic generation [72], and more recently by X-rays reflectivity [80]. The presence

of chains having a significantly different bound fraction implies that the energy landscape of the adsorbed chains can be bimodal, and thus not representative of a system at thermodynamic equilibrium.

Is it possible to equilibrate chains confined in thin films, while they adsorb? Due to the correlation between the kinetics of irreversible adsorption and the time evolution of  $T_g$  during an annealing in the liquid state, we would be tempted to reply no. In fact, reorganization in the adsorbed layer can be so slow that chain degradation occurs before reaching equilibrium. But considering the neat reduction in the growth rate at  $t^* \gg 1$ , we might assume that in this late stage the changes in the dynamics are practically undetectable. Thus we introduced the condition  $t^* \gg 1$  to indicate a steady state mimicking thermodynamic equilibrium, a condition which can correspond to, but is it not strictly bound to, bulk behavior [23].

In the case of melts of PS physisorbed on Al,  $t^*$  has a strong molecular weight dependence, with the adsorption time increasing at larger molecular sizes [23]; on the contrary, for melts of PMMA on quartz [75], and dilute solutions of PS on gold [114], the adsorption rate,  $v$ , see eq. (14), and the onset of the saturation regime,  $h_{\text{ads}} \approx h_{\text{max}}$  see eq. (15), seem  $M_w$ -independent, implying a constant value of  $t^*$  within the experimental limits. This aspect contributes to the non-universality in the adsorption kinetics of polymers onto solid substrate, a feature shared by the deviations from bulk behavior, which further increases the correlation between the two phenomena.

### 3 Scaling of the $\alpha$ -relaxation upon confinement

Molecular dynamic simulations have proven that the impact of interfacial interactions is temperature dependent [115]. In particular, the investigation of dense polymer melts confined between two hard walls [67,115], revealed that the length scale involved in the perturbations of the structural properties introduced by an attractive interface grows exponentially upon cooling. Owing to the correlation between structure and dynamics, a similar scaling was found also for the local dynamics, expressed by  $\tau$  and  $T_g$  [59,66,67,116]. These considerations imply that the effect of a deviation in the dynamics (*e.g.* due to the presence of an irreversibly adsorbed layer) should vanish at sufficiently high temperatures, where the bulk behavior is finally recovered [117,118]. Considering the analogy between temperature and time in relaxation experiments, a bulk-like response is also expected at short observation times, that is, high frequencies or high scanning rates. Indeed, Fakhraai and Forrest proved that the shift in  $T_g$  in ultrathin films depends on the cooling rate, and that larger variations of  $T_g$  are obtained at smaller scanning rates [119]. Similarly, we demonstrated that this trend is consistent with the anomalous response of extremely thin films ( $< 6$  nm) of apolar polymers [19,117], where the electric capacitance increases upon heating, which could hint at a negative thermal expansion coefficient. We rationalized this observation in terms of desorption of polymer chains and thus a larger dipolar activity, upon heating.

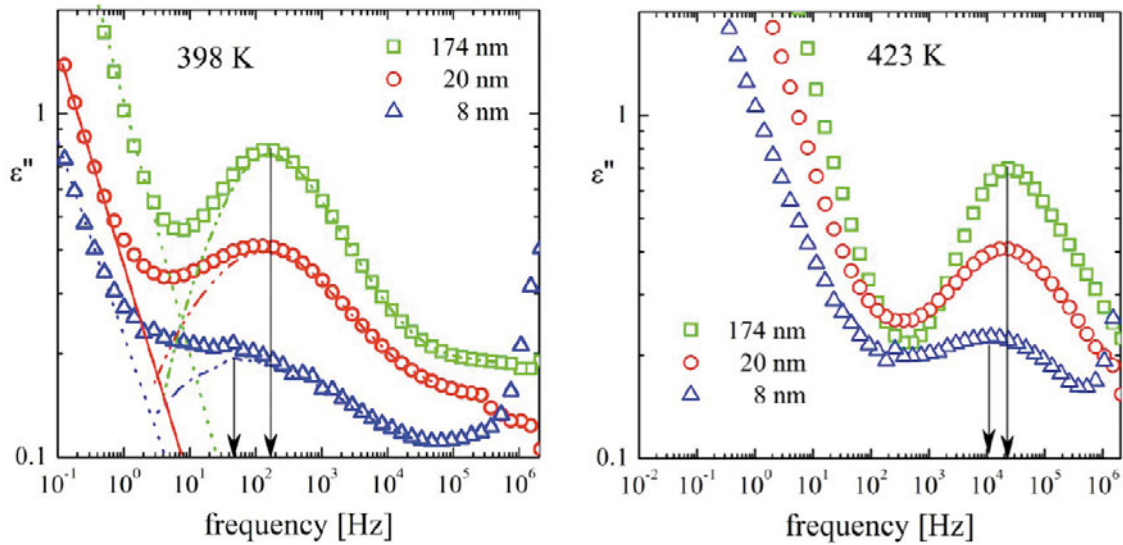


**Fig. 9.** Impact of temperature on the shift in the frequency of the maximum of the structural relaxation of films of different thickness of P2VP-capped Al layers. Note how the separation between the loss peaks reduces at high temperature.

A clear manifestation of these effects in polar polymers is given by the observation that the shift in the  $\tau$  upon confinement gets reduced at higher frequencies, see fig. 9. We could formalize this trend considering the dynamic response of an ideal bilayer system (BULK + adsorbed layer), in which we assumed that the only parameter changing along with the film thickness is the Vogel temperature (or in an equivalent way, the glass transition temperature) [120].

It is noteworthy noticing that our reasoning does not require the introduction of a temperature dependence in the thickness of the adsorbed layer. On the contrary, the effects we describe are related to the temperature dependence of the impact on the global dynamics of a layer of constant thickness, but Vogel temperature different than in bulk. Under these conditions, following a similar scaling proposed for the mode coupling theory [116], the Vogel-Fulcher-Tammann equation can be written as

$$\tau(h, T) = \tau_{\infty} \exp \left[ \frac{BT_0(h)}{T - T_0(h)} \right]. \quad (19)$$

We noticed that the analytical form of eq. (19) resembles other expressions used to characterize the impact of an external force on the temperature dependence of structural relaxation time, where for example the pressure [121], or the degree of polymerization [122] replace the thickness. Such a comparison is justified considering that in the geometry of thin films the inverse of the thickness corresponds to the surface/volume ratio, which indicates the balance between the bulk-like and the interfacial relaxation behavior.

The experimental validity of eq. (19) was confirmed by a careful analysis of the thickness, frequency and temperature dependence of the dielectric function of poly(2-vinyl pyridine), P2VP [120]. The dielectric spectra in isothermal conditions were analyzed in terms of the empirical

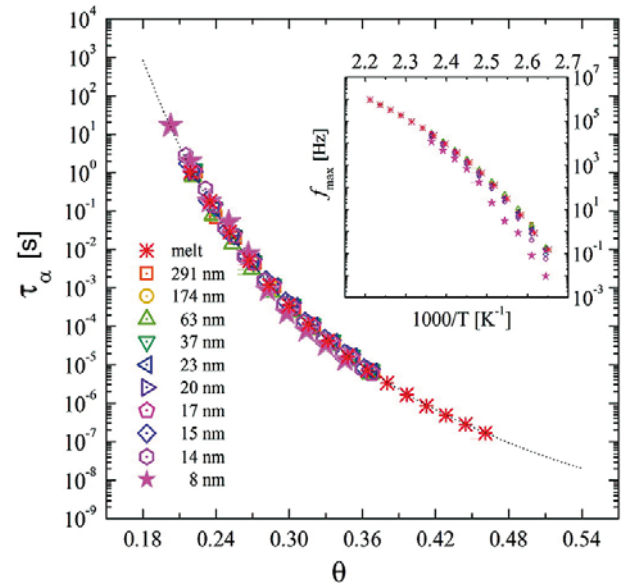


**Fig. 10.** In the inset: frequency of the maximum of the structural relaxation process of the different film thicknesses, as a function of  $1000/T$ . The same curves were superimposed by rescaling the temperature by the dimensionless parameter  $\theta$ , described in the text. Reproduced from Napolitano *et al.* [120] with permission of the American Chemical Society.

HN function, which permitted a reliable and solid determination of the structural relaxation times, also in the case of broad and asymmetric peaks.

Regardless the thicknesses,  $\tau(T)$  followed a non-Arrhenius behavior, see inset in fig. 10. This trend is not in line with what observed in for polymers [123] and low-molecular-weight glass-forming systems confined in nanopores [124], see subsect. 4.2, where a non-cooperative Arrhenius process was observed below a critical volume.

On the contrary, the same behavior of P2VP was found in the majority of the other systems investigated in the geometry of thin films, including glycerol [55]. Consequently we speculate that the trend described by eq. (19) is representative of the scaling of the  $\alpha$ -relaxation under 1D confinement.

As a result of the fits,  $\tau_\infty$  and  $B$  were thickness independent, while  $T_0$  and thus  $T_g$  (which in this case simply reads  $T_0(B/\ln(\tau_g/\tau_\infty))$ , where  $\tau_g$  is the relaxation time at  $T_g$ ) sharply increased for samples thinner than 20 nm. It was thus possible to superimpose all the experimental curves by rescaling the temperature over the dimensionless parameter  $\theta(hT) = T/T_0(h) - 1$ , so that eq. (19) becomes

$$\tau = \tau_\infty \exp(B/\theta). \quad (20)$$

The corresponding master curve is displayed in fig. 10. The physical meaning of our assumptions is evident considering the exponential term of the VFT as the temperature dependence of the activation energy of the relaxation modes involved in the structural process [37]. This is possible by rewriting eq. (20) as  $E_a(T)/k_B T = B/\theta$ , which implies that a higher value of the Vogel temperature corresponds to higher effective activation energy for the structural relaxation. Consequently the increase of  $T_0$  observed upon thickness reduction for ultrathin films of P2VP reveals an increase in the potential wells, reducing the probability for rotational jumps in the adsorbed layer. In line with our findings on the reduction of  $T_g$ , we propose that such a higher barrier is the effect of a reduction of free volume (densification) in proximity of the metallic interface, yielding a larger correlation between monomers, and an enrichment in the population of relaxing units (here, dipole moments) associated to slower relaxation modes. The positive value of  $\Delta T_g$  is thus related to a higher value of  $T_0$  in proximity of the adsorbing interface [125]. Analogously, simulations have shown how the potential energy minima connected to the different relaxation modes are deeper for the molecules in proximity of an attractive interface [67].

The feasibility of the scaling of  $\tau(h, T)$  over  $\theta$  provided new insight on the potential energy landscape (PEL) of chains in the adsorbed layer. Considering the small variation of  $T_0$  ( $< 2\%$  at 8 nm), we speculate that the shape of the PEL of the adsorbed layer is not particularly different than in bulk, which is consistent with the evidence that, except in a few cases [70,126], the dynamic fragility,  $m_p$ , does not depend on the film thickness. Under the conditions validating our scaling ( $B$  and  $T_g/T_0$  constant), in fact, we obtain

$$m_p \equiv \left. \frac{\partial \log \tau}{\partial (T_g/T)} \right|_{T=T_g} = \frac{B}{\ln 10} \frac{T_g/T_0}{(T_g/T_0 - 1)^2} = \text{const.} \quad (21)$$

This reasoning implies that the relaxation of glass-forming systems in proximity of an adsorbing interface requires the same mechanism as in bulk, as remarked for example by Ngai [127]. Moreover, the validity of eq. (20) implies that it is always possible to relate the relaxation rate of a thinner film to that of a bulk sample at lower temperatures, that

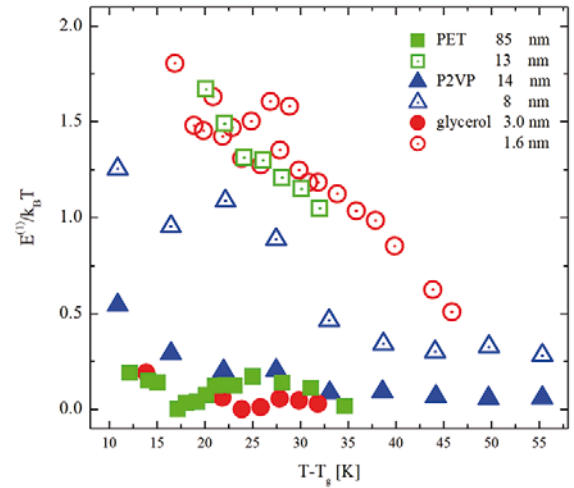


**Fig. 11.** Confinement energy for PET, P2VP and glycerol as a function of the distance from  $T_g$ .

is, the increase in relaxation time in proximity of a solid interface has the same molecular origin as the increase in relaxation time upon cooling. This idea is in line with the prediction of the TOP model, explaining the slower interfacial dynamics similarly as for vitrification upon cooling, in terms of an increase in interparticle correlations, not driven by changes in density [39].

With these considerations in mind, we treated substrate interactions as small perturbations on the value of the Vogel temperature,  $\delta T_0$ , which yields, at the first order, a correction factor in the activation energy,  $E^{(1)}(T)$ . We demonstrated that it is possible to build up this parameter, starting from experimentally achievable quantities

$$\begin{aligned} \Delta(h, T) &= \ln \left[ \frac{\tau(h, T)}{\tau(\infty, T)} \right] = \frac{|E(h, T) - E(\infty, T)|}{k_B T} \\ &\approx \frac{E^{(1)}(h, T)}{k_B T}, \end{aligned} \quad (22)$$

where with  $\infty$  we indicate the unperturbed response of a bulk system. In fig. 11 we plotted the values of  $\Delta(h, T)$  for ultrathin films of different polymers and of the low-molecular-weight glass-former glycerol. Thinner samples show higher values of  $\Delta(h, T)$ , but, regardless of film thickness, the confinement effects reduce upon heating, as expected [119,125].

In subsect. 4.5, we describe a method to determine the length scale of interfacial interactions,  $\varphi$ , based on the thickness dependence of the contribution of the orientational polarization to the dielectric constant [65]. When the thickness dependence of the dielectric strength was available at different temperatures, we could analyze the impact of supercooling on the mobility profiles, and verify that even in this case the deviation from bulk behavior showed the expected temperature dependence.

The results of the computations, summarized in fig. 12, confirmed a reduction of the penetration depth of the interfacial interactions upon heating, manifesting as smaller

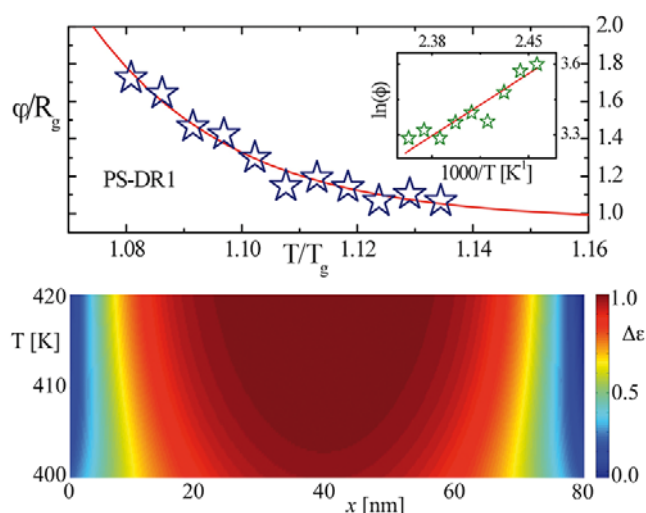


**Fig. 12.** Temperature dependence of the penetration depth of the dielectric strength  $\varphi$ , normalized to the radius of gyration  $R_g$  ( $\sim 25$  nm), for PS-DR1 (top panel); the red curve is a smooth function used as guide for the eyes. The same smooth function was used to obtain the temperature dependence of the local dielectric strength  $\Delta\varepsilon(x, T)$  for an 80 nm thick film (bottom panel). Reproduced from Rotella *et al.* [65] with permission of the Royal Chemical Society.

values of  $\varphi$  when the temperature of the polymer melt is raised. In the limit of high temperatures,  $T > 1.15T_g$ ,  $\varphi$  approaches the gyration radius while extrapolation at  $T_g$  confirmed that in a deeply supercooled melt the  $R_g$  is not the largest length scale characterizing the size of the interfacial region. In fact, already at  $1.07T_g\varphi > 2R_g$  and at  $T_g$   $\varphi$  might exceed by ten times the molecular size.

Our results could finally validate the prediction of previous molecular dynamic simulations [115], where the growth of the length scale of the perturbations in the dynamics introduced by an interface increases exponentially upon cooling, with an activation energy weaker than that of  $\tau$ , that is  $d \ln \varphi / d(T^{-1}) < d \ln \tau / d(T^{-1})$ . In particular, for labeled polystyrene (PSDR1), we found that the thermal activation barrier of  $\varphi$  is  $35 \pm 2$  kJ/mol, *i.e.* 6–7 times smaller than the activation energy of the structural relaxation time in the same temperature range [11], while for polycarbonate we obtained values 10 times smaller [71]. This implies that a small variation in the structure produces larger effects on the dynamics, as observed also in bulk. At the molecular level, we speculate that the electric polarization can sense this phenomenon because of a reduction in the preferential orientation of the dipole moments in the adsorbed layer upon heating, which results in a virtual thinning at higher temperatures.

#### 4 Gradients of structural relaxation under 1D confinement

A general feature of the dynamics upon confinement is the manifestation of a gradient of mobility introduced by the presence of interfaces. Molecular motion at the

very interface with air (or vacuum) is facilitated by different molecular configurations arising from surface ordering and an intuitive increase of free volume. On the contrary, a slower dynamics is encountered in the case of densely packed chains due to the lesser space available for molecular motion. These perturbations propagate towards the core of the film and die out gradually with the distance from the interface, giving rise to a smooth gradient of relaxation times, or equivalently to a distribution of glass transition temperatures [89]. Such a gradient revealed by molecular dynamics simulations was confirmed by several experimental approaches. In particular, by placing a (fluorescent) dye-labeled polymer layer at a specific position within a stack of unlabeled polymer layers, Ellison and Torkelson could determine a volumetric glass transition temperature averaged over a depth region of typically 15 nm [128]; as an outcome of this experiment, the authors determined that, for PS, the effects of free surfaces on the reduction in  $T_g$  covers 30 nm. By monitoring the embedding of gold nanospheres onto surfaces of PS, Fakhraai and Forrest verified that the segmental mobility of a 2 nm surface layer is enhanced by more than 10 orders of magnitude in comparison to the bulk [17]. Dinelli *et al.* indicate a similar upper limit for the region with different viscosity on top of supported films of PS [129, 130]. In the case of solid interfaces, much larger length scales seem to be involved. Rittingstein *et al.*, found, for example, that the increase in  $T_g$  in nanocomposites of silica in P2VP can arrive up to interlayer spacings of 500 nm [98]; while Koga *et al.*, by measuring the viscosity of thin films of PS99, verified that free surface can “feel” the presence of an irreversibly adsorbed layer up to 50–60 nm [131], that is about  $6R_g$ . Regardless of the different penetration depths reported in the literature, the manifestation of a gradient of mobility is ubiquitous.

#### 4.1 Broadening of the structural peak as seen by dielectric spectroscopy

In our work, we aimed at verifying whether also the  $\alpha$ -relaxation feels the presence of such a gradient and what is its molecular origin. In their seminal work on the use of dielectric spectroscopy in the investigation of ultrathin polymer films, Fukao and Miyamoto observed a broadening of the structural peak of films of PS capped between Al layers, increasing upon reduction of the film thickness [15]. Serghei and Kremer, noticed that the shape of the structural peak of samples probed by their apparatus for supported films (see subsect. 1.2.2) is not affected by the reduction of the layer thickness. Claiming that the structural relaxation does not feel the effects of confinement, they suggested that the broadening reported in capped films is instead imputable to the presence of the aluminum electrodes [132]. On the contrary, Nguyen *et al.* investigated poly(vinyl acetate) by local dielectric spectroscopy and reported a broadening following the same phenomenology as in capped films [32]. Similarly, in multilayers experiments we found a distribution in  $T_g$  and  $\Delta\varepsilon$  [11], and using IDE we detected a thickness dependence in the shape

parameters of thin glycerol films, and in the widths of the  $\alpha$ -peak of freely standing films of PS [133]. Thus, we can conclude that the broadening in the  $\alpha$ -peak is a genuine effect, given by the effect of interfaces on the distribution of relaxation times.

The (asymmetric) broadening of the  $\alpha$ -peak upon confinement was often interpreted in terms of the effect of spatial heterogeneity on the dynamics, which yields larger distributions of relaxation times. By means of the HN function and the formalism introduced by Schönhals and Schlosser [44], it is possible to quantitatively analyze the changes in the structural peak, relating the limiting slopes of the  $\alpha$ -process in a plot of  $\log(\varepsilon'')$  vs.  $\log(\omega)$  to the shape parameters  $a$  and  $b$ : for  $\omega \ll 1/\tau_{\text{HN}}$ ,  $\varepsilon'' \sim \omega^m$  and  $\varepsilon'' \sim \omega^{-n}$  for  $\omega \gg 1/\tau_{\text{HN}}$ , where  $m = a$  and  $n = ab$ . We remind that a reduction in  $a$  corresponds to broader peaks, while the asymmetry is revealed by smaller values of  $b$ . For polymers in bulk,  $n$  varies between 0 and 0.5, differing sensitively from the behavior of low-molecular-weight glass formers where  $n$  can approach 1 at relatively high temperatures. The limiting condition  $n = 1$  can be reached in the case of a Debye relaxation, where the whole dispersion width is due to one single relaxation time. In this particular case, the  $\alpha$ -peak has already an intrinsic full width at half-maximum (FWHM) extending for more than 1 decade.

It is tempting to assume that a perturbation in the dynamics associated to enrichment in slower relaxation modes, *e.g.* chain immobilization, or an increase in  $T_g$ , will result in a reduction in  $m$ , while a change in  $n$  could be linked to the fast dynamics (free surface, or excess of free volume). However, application of these intuitive concepts might not be so straightforward. Severe criticism to this approach comes from the idea that in bulk the shape of the  $\alpha$ -process is not directly related to a distribution of relaxation times arising from spatial heterogeneities. In fact, the symmetric and asymmetric broadening of the  $\alpha$ -peak should be instead considered as a characteristic feature of the dynamical glass transition and the low- and high-frequency limiting slopes of the dispersion process should be associated to the motion of the chains at, respectively, larger and smaller length scales [43]. Though derived from an empirical function, the value of  $n$  and  $m$  can be formally correlated to the mechanism originating the structural relaxation. For bulk polymer systems, the segmental dynamics is influenced by the motions of the neighbored segments: the damped diffusion of conformational states described for dilute polymer solutions is here replaced by a hindered mechanism. Considering a model system with 2 conformational states marked as 0 and 1 (as *trans* and *gauche* conformations), the probability  $\psi$  that at a given time  $t$  the segment corresponding to the spatial variable  $x$  is in the state 1 is given by [44]

$$\frac{\partial \psi(x, t)}{\partial t} = -\frac{1}{\tau_0} \psi(x, t) + \int_0^t \frac{\partial D_C(t - \tau)}{\partial t} \frac{\partial^2 \psi(x, t)}{\partial x^2} d\tau, \quad (23)$$

where  $\tau_0$  is a time constant of the transition between conformational states (in equilibrium with the thermal bath) and  $D_C$  is the diffusion coefficient of the conformational

states. The hindered damped diffusion regime is ensured by assuming  $\partial D_C / \partial t \sim t^{-\lambda}$ , being  $|\lambda| \leq 1$ .

By limiting to the cases corresponding to  $-1 \leq \lambda \leq 0$  (diffusion in inhomogeneous media related to a continuous random walk) it is possible to link the value of the exponent  $\lambda$  to the high-frequency limiting slope of the dielectric loss, as  $n = (1 + \lambda)/2$ . The value of  $n$  is thus a probe of the local dynamics. Upon cooling, chains pack more efficiently and segmental dynamics is more hindered. As a consequence,  $n$  assumes smaller values at lower temperatures, that is, the  $\alpha$ -peak broadens on the high-frequency side. Similarly, at high temperatures, the augment of free volume leads to an increase of  $n$ , that is, a sharpening of the relaxation peak. The value of  $m$  appears instead to be related to fluctuations taking place at length scales larger than those characteristics to the structural dynamics. This consideration is supported by the fact that crosslinking affects only  $m$ , and that in semi-rigid polymers like PET [134], during crystallization  $n$  remains constant, while  $m$  changes sensitively. Furthermore, for more flexible polymers as poly(3-hydroxybutyrate) (PHB), both shape parameters remain unaltered [81, 135, 136], implying the lack of long-range effects in the perturbation of the  $\alpha$ -relaxation upon crystallization in these systems.

Applying similar arguments to the broadening observed in thin polymer films yields non-intuitive trends. In fact, an increase in polarization at frequencies larger than the mean relaxation time, detectable as a reduction in  $n$ , could be interpreted as both an enrichment in faster relaxation modes corresponding to a lower effective  $T_g$  (“spatial heterogeneity” hypothesis) and as an increased hindrance in the local chain dynamics leading to a higher effective  $T_g$  (“bulk scaling” hypothesis). A recent experiment permitted us to discern between the two explanations and validated the spatial heterogeneity approach [23]. The value of  $n$  for 20 nm thick capped films of PS increased at larger degrees of adsorption. According to the bulk scaling, such a trend should correspond to an increase in free volume, and a concurrent possible drop in  $T_g$ . On the contrary, the interfacial free volume drops upon adsorption, validating our hypothesis on the spatial heterogeneity. Consequently, it is possible to use the changes in the shape parameters of the  $\alpha$ -relaxation to extract direct information on the gradient of mobility.

In the following section we show three different methods to estimate the gradients of mobility in ultrathin films of polymers and low-molecular-weight glass formers based on the analysis of their dielectric function.

#### 4.2 Enslaving free surfaces to the dynamics in proximity of a solid interface: the case of thin films of glycerol on quartz

We investigated the molecular dynamics in supported thin films of glycerol by means of interdigitated comb electrodes [55]. Measurements performed during slow desorption at 230 K ( $= T_g + 36$  K), down to a single molecular layer ( $\approx 0.7$  nm), permitted to verify the existence of a layer with enhanced mobility in the vicinity of the free

surface, enslaved to the slower dynamics of the molecules sitting at the interface with the quartz substrate. Films as thin 1.6 nm were analyzed over a broad range of time scales ( $> 6$  decades). We did not observe any transition from cooperative to single molecule dynamics, that is, from super-Arrhenius to Arrhenius, as instead observed in silica matrices with 2.2 nm pores [124]. Consequently, in our analysis, we discarded finite-size effects arising from mere geometrical constraints and focused on the impact of interfacial interactions on the shape of the  $\alpha$ -peak. For films thinner than 50 nm, we observed an asymmetric broadening accompanied by a slowdown in the dynamics when the thickness was reduced to 2 nm, expressed by shift in the Vogel temperature by +5 K and a corresponding increase of  $T_g$  by 3.5 K. These trends suggested the mobility of molecules in the first couple of layers in close proximity of the substrate is reduced in comparison to the bulk (reduced mobility layer, RML) [16]. We attributed this trend to the H-bonding interactions between glycerol and the substrate of the IDE sensor.

In addition to this minor variation in  $\tau$ , we expected that the presence of interfaces could cause an increase in the dynamic heterogeneity of the system. As the RML and the free surface induce opposite effects on the molecular dynamics, we proposed that it was possible to distinguish their particular contributions by means of the “shape” parameters  $m$  and  $n$ . In this formalism, reductions in  $m$  or in  $n$  reflect respectively, an enrichment of the distribution of relaxation times at long time scales (slower dynamics) induced by the presence of a reduced mobility layer (RML) or at short time scales (faster dynamics), by a free surface, or an enhanced mobility layer (EML).

Since we are not dealing with polymers, we modeled our films as trilayers, where a bulk-like region is embedded between reduced mobility layer (RML) in proximity of the solid interface and an enhanced mobility layer (EML) at the free surface. The impact of the bulk component is expected to decrease upon thickness reduction, resulting in an increase in  $m$ , in case the slower dynamics of the RML were dominant, or an increase in  $n$ , if the dynamics of the whole film were accelerated by the EML.

Figure 13 shows the thickness evolution of the values of  $m$  and  $n$  obtained from spectra acquired during continuous desorption experiments. Up to thicknesses on the order of 50 nm, the values of both  $m$  and  $n$  are intrinsically lower than those obtained for bulk glycerol probed with an isotropic electric field; this apparent discrepancy was actually predicted by molecular dynamics simulations of the effect of an electric field on the dielectric response [59].

In the same figure we plotted also the value of the relaxation time, to ease the comparison between peak shape and the evolution of the dynamics. For bulk glycerol, in the temperature range from 197 to 237 K,  $\tau$  changes by more than 6 orders of magnitude, while the values of  $m$  and  $n$  have a very weak temperature dependence [137, 138]. On the contrary, here we found severe changes in the shape parameters, while the value of  $\tau$  was almost constant. It is noteworthy noticing that a given increment in  $m$  or  $n$  is not linearly correlated to the resulting increase in the width of the relaxation peak. Remarkably, small varia-

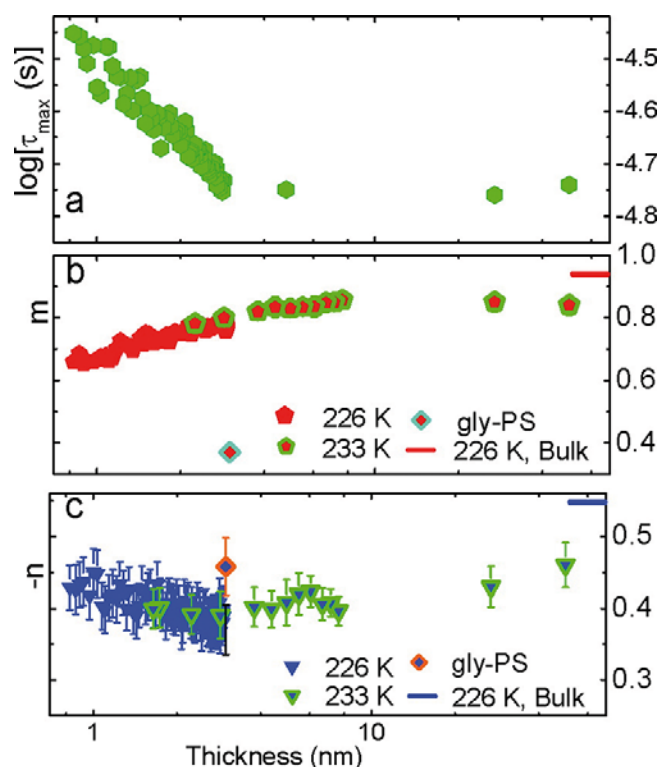


**Fig. 13.** a) Thickness dependence of the structural relaxation time, measured during isothermal desorption at 226 K. b) and c) Parameters  $m$  and  $n$  obtained from two distinct measurements during isothermal desorption: at 233 K, in the thickness range between 2.5 and 8 nm, and at 226 K, between 3 and 0.7 nm. Reproduced from Capponi *et al.* [55], with permission of the American Chemical Society.

tions in the  $m$ , or  $n$ , provide a tremendous broadening of the peak that permits an accurate determination of the value of the shape parameters. Below 3 nm the relaxation time gets longer, while the value of  $m$  decreases already at 6–8 nm. Thus the increase in  $\tau$  is caused by a more pronounced dielectric response at low frequencies, *i.e.* a larger impact of the RML on the relaxation dynamics of the system upon thickness reduction. The absolute value of  $n$ , on the contrary, decreases already at few tens of nm, shows a broad minimum centered on 3 nm and it finally recovers “bulk” values below 1 nm. The different thickness dependence of the two shape parameters implies asymmetric peak broadening upon film thinning. Thus, changes of  $m$  and  $n$  are caused by a variation in distribution of the relaxation times rather than by an intrinsic increase in the heterogeneity caused by confinement, which would instead induce a symmetric broadening.

In addition to this expected trend, a finer analysis of  $m$  and  $n$  suggested that in thinner films, the reduction of the bulk component pushes the free surface towards the RML and the EML gets enslaved to the slow dynamics. In fact, while the reduction in  $m$  is detectable already in films as thin as 50 nm, the opposite effect is observed below 3 nm. In this thickness range,  $\tau$  increases and the more stable boundary conditions imposed by -OH bonding with

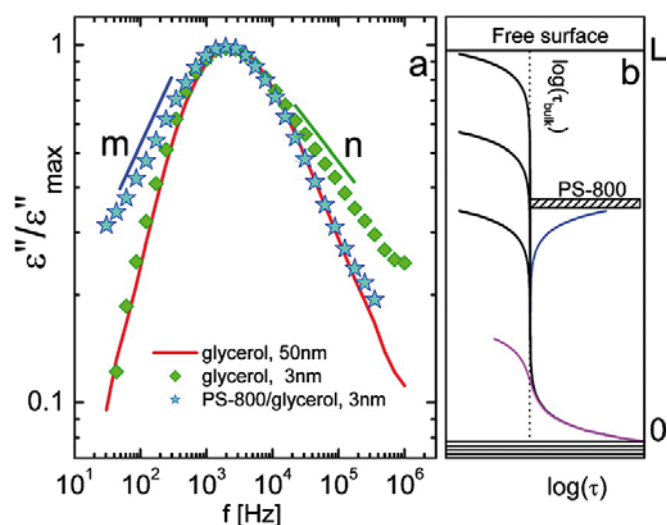


**Fig. 14.** a) Dielectric loss curves acquired for a 3 nm glycerol film at 217 K, before and after capping with PS0.8 compared with a 50 nm thick film (blue line). b) Sketch of mobility profiles across the film, for different values of the total thickness. The blue curve represents the profile in a capped film. Reproduced from Capponi *et al.* [55], with permission of the American Chemical Society.

the quartz substrate inhibit the action of the EML. This reasoning is consistent with the experimental evidence collected by Torkelson and coworkers, suggesting that the glass transition of a free surface is enslaved to the nature of the underlying layer [139].

To further validate these ideas, we designed other experiments, which permitted to achieve more information on the contribution of regions with faster dynamics in glycerol and their impact on the structural relaxation. For this purpose, we measured the response of a capped film (fig. 4a), where the free surface of a 3 nm thick film of glycerol was suppressed by the presence of a layer (9 nm) of low-molecular-weight polystyrene ( $M_w = 800$  g/mol,  $T_g = 269$  K). We chose this oligomer because it does not present any relaxation process in the chosen temperature range, consequently any difference in the relaxation pattern of the two measurements could be attributed to a different nature of the interfaces. Moreover, as the temperature range of our investigation was kept below the  $T_g$  of PS, the extremely low miscibility with glycerol ensures geometrical stability of the system for the whole duration of the experiment.

Spectra of the capped film were acquired upon heating, and compared to measurements performed on the underlying glycerol layer before capping. Figure 14 displays loss curves acquired at 217 K for both the capped and the uncapped film. The comparison between the dielectric spectra before and after capping revealed a depletion of faster molecules in the capped film. In fact, as expected, an additional RML appeared at the upper interface, consisting with the lower value of  $m$  upon evaporation of PS onto the free surface of glycerol. In addition to this feature, we observed relaxation times exceeding the bulk value and a

non-zero value of confinement energy  $\Delta(h, t)$  at thicknesses larger than in the case of supported films. In fig. 14a we reported for comparison the loss curve measured at the same temperature for an uncapped 50 nm thick film. The relaxation peak of the 3 nm capped film overlaps the high-frequency component of the peak of the thicker film, where we expect that the EML has no impact on the overall molecular mobility. This evidence proves that the free surface is suppressed by depositing a capping layer. Based on the experimental evidence in, we sketched fig. 14b possible mobility profiles capturing the concurrent effects of a RML and an enhanced mobility layer on the overall dynamics

The suppression of the free surface results in a reduction of the relaxation peak component at high frequencies by a component whose dielectric strength corresponds roughly to one fourth of the overall signal of the uncapped glycerol film. A crude analysis of this information reveals that, for glycerol, the effects of the free surface on the structural dynamics are limited to a monolayer. The small extension of the EML and the increasing values of  $n$  in the thinner film prove that faster dynamics of the free surface is enslaved to the slower relaxation modes of the RML, which rationalizes the slowdown of dynamics observed below 1.6 nm.

### 4.3 Asymmetric broadening in freestanding films of PS

In addition to the reduction in the glass transition temperature detected by ellipsometry [140], Brillouin light scattering [141], fluorescence spectroscopy [142], dielectric spectra of freely standing films of PS revealed new intriguing features [133]: a temperature-dependent asymmetric broadening of the  $\alpha$ -peak towards lower temperatures and a reduction of the dynamic fragility down to the monomer limit. A fine analysis of our experimental results confirmed the presence of a strong gradient of  $T_g$ 's extending inside the film.

During relaxation and retardation experiments, thermally activated processes appear as peaks in both the frequency and the temperature dependence of the imaginary part of the chosen susceptibility [41]. In the case of freely standing films of PS, it was possible to analyze the asymmetry and the thickness-dependent broadening in the  $\alpha$ -peak, in isochronal plots. This approach, reproducing temperature scans at constant heating/cooling rate, allowed direct comparison of our results with those collected under similar experimental conditions, *e.g.* via ellipsometry. The complex electric capacitance of freely standing films of atactic PS ( $M_w = 932000$  g/mol,  $M_w/M_n = 1.2$ ) was measured using a high-resolution dielectric analyzer under high vacuum, in the temperature region from above the bulk glass transition down to room temperature and in the frequency domain from 1 Hz to 1 MHz. Integrity of the samples and their freely standing character after several heating cycles above bulk  $T_g$  were confirmed by atomic force microscopy [53].

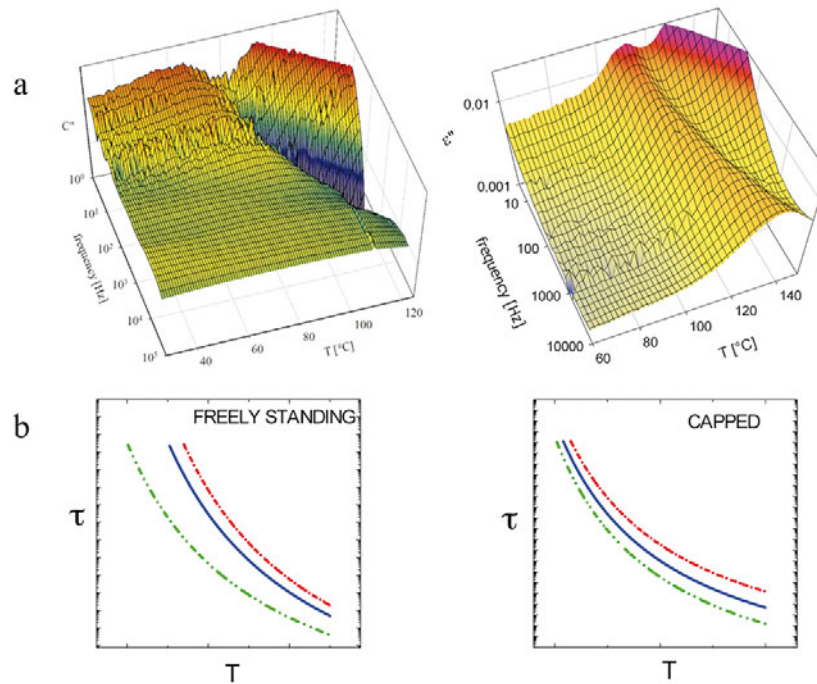


**Fig. 15.** (a) Comparison between the frequency and temperature dependence of the imaginary part of the complex capacitance of a 40 nm thick freely standing membrane of PS (932000 g/mol) and the dielectric loss (scaling with the capacitance via a geometrical factor) of a 45 nm thick film of PS (932000 g/mol) capped between aluminum electrodes. (b) Sketch of the temperature dependence of the structural relaxation time (blue) and of the peak broadening; green and red lines respectively indicate the onset and the offset of the  $\alpha$ -peak. Reproduced from Napolitano *et al.* [133] with permission of Elsevier.

#### 4.3.1 Gradient of $T_g$ 's

Figure 15 shows a 3-dimensional plot of the typical response of  $C''(f, T)$  in freely standing films, where a single relaxation process is present. By comparison with the values of  $T_g$  in the thinner layers, and by its dynamic fragility in the thicker films, we attributed this peak to the structural relaxation of PS. In the FSF geometry, the activation energy of the process ( $E_a$ ) increases upon cooling, resulting in a pronounced bend of the peak maxima towards lower frequencies at lower temperatures. This trend arises from the strong increase in activation energy of the structural process in proximity of the glass transition and is a common feature of the glassy dynamics. The tremendous asymmetric broadening of the peak is, however, surprising.

The relaxation scenario in FSF substantially differs from what typically observed in bulk samples, see fig. 15. At lower frequencies, the low-temperature tail of the  $\alpha$ -peak extends well below room temperature. For a 225 nm thick membrane, in an isochronal representation at 4.5 Hz, the FWHM reaches 56 K, see fig. 16, a value that reduces to 35 K at 300 Hz. Differently from what is seen in capped films, the broadening increases with the film thickness and is always less pronounced in the high-frequency region. On the contrary, in bulk samples, the structural relaxation peak of PS is symmetric with a FWHM of 17 K at 4.5 Hz, a value increasing to 24 K at 300 Hz. Such a behavior is noteworthy different from what observed in

nanolayers of PS confined between solid interfaces, where the broadening is athermal and more relevant at higher surface/volume ratios [15].

Given the distribution in relaxation times, the width of the  $\alpha$ -peak in isochronal representations is bound to the activation energy of the molecular processes involved. Sharper peaks correspond to higher values of  $E_a$ , that is, at given frequency the relaxation process affects the susceptibility within a smaller temperature window; in other words, at constant heating (cooling) rate, a process with higher activation energy will span the experimental accessible frequency range faster than a process with lower  $E_a$ .

At temperatures just above  $T_g$ , a modest reduction of the temperature corresponds to a progressive increase in the viscosity and thus in the mean value of  $\tau$  [36]. As a consequence, the activation barrier for rotational jumps increases upon cooling, and the  $\alpha$ -peak sharpens in isochronal representations at lower frequencies. With this reasoning in mind, we should think that a large drop in the activation energy upon cooling is responsible for the broadening observed in the structural peak of FSFs in the proximity of  $T_g$ . This conjecture has no physical basis and it would not justify the large asymmetry of the peak.

On the contrary, we verified that the trends found for the maximum of the  $\alpha$ -relaxation and its peak shape are clear manifestations of a gradient of glass transition temperatures induced by an enhanced molecular mobility at

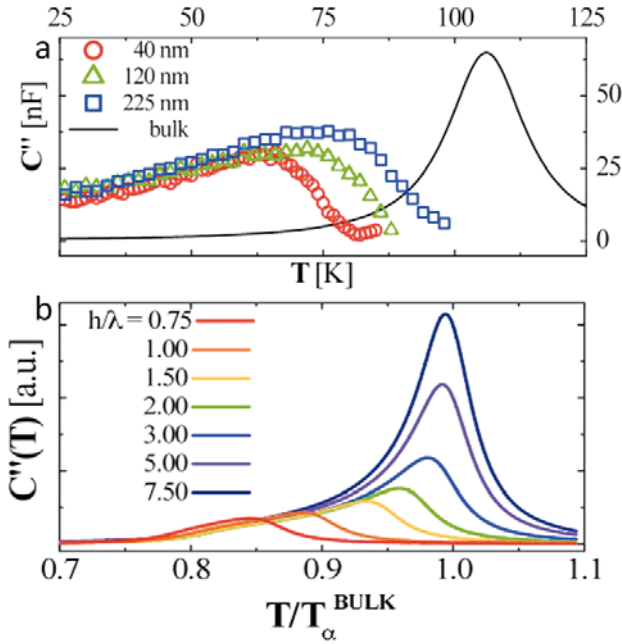


**Fig. 16.** (a) Isochronal representation ( $f = 4.5$  Hz) of the imaginary part of the complex capacitance for freely standing films of PS of different thickness. A peak of arbitrary intensity but the same peak maximum and full width at half-height as for bulk samples has been added for comparison. (b) Isochronal representation of the imaginary part of the complex capacitance computed via eq. (25). Reproduced from Napolitano *et al.* [133] with permission of Elsevier.

the two free surfaces of the freely standing film [12,128]. Ellipsometric measurements in supported films of PS by Kawana and Jones [143] support the existence of a similar asymmetric broadening in the structural relaxation where free surfaces are characterized by lower transition temperatures; similar trends were recently revisited by Kim *et al.* [142]. We could rationalize the phenomena observed in the spectra of freely standing films translating recent experimental and theoretical observations into an equivalent dielectric response, obtained by modeling free surfaces as potential barriers imposing an exponential decay of the relaxation temperature [59,66,116]. To compute the dielectric response of a membrane, we assumed that each sublayer of unitary thickness could be schemed as a bulk-like peak. Given the geometry of the film, we introduced a profile of the position of the maxima of the structural peak in isochronal representations,  $T_\alpha$ , symmetric with respect to the center of the film, which mimics a smooth gradient in  $T_g$

$$T_\alpha(x) = T_\alpha^{\text{BULK}} \left[ 1 - \exp\left(-3\frac{x}{\lambda}\right) - \exp\left(-3\frac{h-x}{\lambda}\right) \right], \quad (24)$$

where  $T_\alpha^{\text{BULK}}$  is the value of the relaxation temperature in bulk and  $\lambda$  is the length scale necessary to cancel the surface effects. Considering eq. (24), the deviation from

the bulk behavior at distances on the order of  $\lambda$  from each interface is limited to 5%,  $\exp(-3) < 0.05$ . To obtain the contribution,  $\Delta x^i$ , of each sub-layer we sampled the values of  $T_\alpha$  with a fixed step  $\Delta T_\alpha$ , which we used as weight coefficients

$$C'(T) = C_0 \sum_i \frac{\Delta x^i}{1 + [2\Phi(T - \bar{T}_\alpha^i)]^2}, \quad (25)$$

where  $C_0$  is the value of the geometrical capacitance of the measurement cell per unit of thickness,  $\Phi$  is the FWHM of the structural process in bulk,  $\Delta x^i$  and  $\bar{T}_\alpha^i$  are, respectively, the thickness and the average relaxation temperature of the  $i$ -th layer. The procedure described by eq. (25) is equivalent to averaging the contribution of each layer, via its volume fraction. In line with our experimental trends, the results of our computation show a reduction in peak width upon increase of the thickness, see fig. 16. Films much thicker than  $2\lambda$  have a bulk-like response, that is  $T_\alpha = T_\alpha^{\text{BULK}}$  and  $\text{FWHM} \sim \Phi$ .

Upon reduction of the sample size (here expressed by the dimensionless parameter  $h/\lambda$ ), the presence of interfacial layers becomes more relevant, and their contribution to the dielectric relaxation shows up as a tail in the low-temperature region. In this regime  $T_\alpha$  decreases, while FWHM increases. When the confinement size reaches  $2\lambda$ , due to the mutual effect of the two opposing free surfaces, the film does not contain any bulk component, and a further reduction of the thickness yields a cutoff of bulk-like relaxation modes. Consequently the distribution of relaxation times is limited to the fast surface modes, the  $\alpha$ -peak narrows and the FWHM inverts its trend and decreases. Our reasoning is in line with the model on the propagation of free volume proposed by Lipson and Milner [33], and the experimental evidence by Torkelson and coworkers, both suggesting that films thinner than the double of the perturbation length scale introduced by a free surface cannot sustain the full gradient of glass transition temperatures [142,144]. A crude comparison between our results and the computation revealed values of  $\lambda \sim 150$ – $200$  nm, a value which exceeds by one order of magnitude the value proposed by Paeng *et al.* [145], but similar to the penetration depth induced by substrate interactions (silicon and aluminum oxide) on the relaxation time of free surfaces of isotactic PMMA ( $\sim 180$  nm) [30]. A possible source of discrepancy could be related to the averaging procedure present in eq. (25), as it does not take into account a possible distribution in orientational polarization which might arise from the increase in interparticle chain ordering. We recently verified that the imaginary component of the capacitance increases in proximity of interfaces, due to a larger local value of the Kirkwood correlation factor [57], which is a probe for the degree of correlation among dipole moments. Consequently, the contribution of interfacial layers to the final value of the capacitance might be overestimated, and the effective value of  $\lambda$  results lower. Further investigation on this topic will provide deeper insight on the chain structure in freely standing films.

### 4.3.2 Gradient of activation energy: From cooperative to non-cooperative dynamics

The anomalous narrowing of the peak in the high temperatures/high frequencies region can be explained considering a reduction of the deviations from bulk behavior (*e.g.*  $\lambda$ ) at higher temperatures, (see sect. 3). Due to the intrinsic form of the temperature dependence of  $\tau$ , the differences between  $E_a$  of each sub-layer increase upon cooling, leading to the characteristic diverging shape seen in the 3D representation of the loss spectra, see fig. 15. Moreover, the thickness dependence of the changes in  $E_a$  upon cooling strengthens the idea that the broadening observed in thin films is connected to the dynamic heterogeneity. We extracted the temperature dependence of the structural relaxation time out of 3D representations assigning the traces of the process to those couples of frequency and temperature values ( $f_{\max}, T_\alpha$ ) identifying the maximum of the structural relaxation peak, see subsect. 1.1. For all the thicknesses investigated the temperature dependence of  $\tau$  could be fitted by the Vogel-Fulcher-Tammann equation. The increase of  $\tau$  upon temperature reduction was quantified in terms of the dynamic fragility, see eq. (21). The values of  $m_p$  decrease in the thinner films and surprisingly the value of the fragility of 40 nm thick membranes crosses the monomer limit [146]. This intriguing result suggests that the surface dynamics of polystyrene does not share the same cooperative nature of its structural relaxation in bulk and its impact on the properties averaged over the whole membrane is enormous. Our results are in line with the transition from cooperative to non-cooperative behavior in the temperature dependence of the viscosity of supported PS films, found by Yang *et al.* upon reduction of the thickness [29], and the smaller values of  $m_p$  revealed by Priestley and coworker in nanospheres of PS at larger surface/volume ratios [147].

### 4.4 Gradient of segmental mobility and orientational polarization strength via a multilayer approach

In the case of supported films, inspired by the approach proposed and exploited by Torkelson and coworkers based on fluorescence techniques [128], we took advantage of the sensitivity of dielectric spectroscopy and determined the gradients of structural relaxation time and orientational polarization in capped polymer films [11]. In addition to the information achieved on the depth profile of  $T_g$ , the investigation of the dielectric function over a large frequency range permitted to map the segmental mobility also by means of the dielectric strength, a quantity proportional to the amount of mobile molecules relaxing on the time and the length scale of the dynamic glass transition. The possibility to enhance the dielectric response of nearly apolar polymers by doping it with molecular dipoles that are either dispersed (probes) or covalently attached to the polymer chain (labels) was previously validated in bulk systems [148] and finally extended to ultrathin polymer films [149]. In order to reduce the inter-diffusion depth between consecutive layers and to achieve

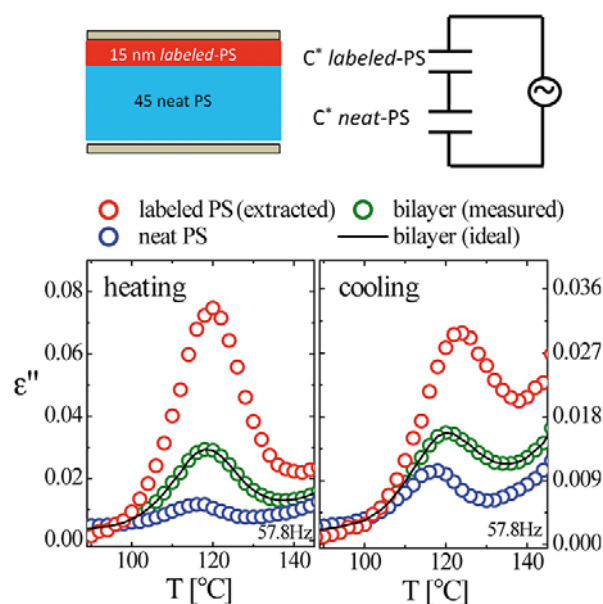


**Fig. 17.** On the top, scheme of a bilayer composed of a 45 nm thick film of neat PS surmounted by a 15 nm thick layer of l-PS and corresponding electric circuit. On the bottom isochronal representation (57.8 Hz) of the imaginary part of the dielectric permittivity of the bilayer described above. The permittivity of l-PS was obtained upon subtraction of the complex capacitance of the layer of neat PS previously measured. The ideal response of the bilayer was computed upon addition of its components, to verify the solidity of our approach.

sufficient contrast in the dielectric signal, it was necessary to synthesize a high-molecular-weight PS where 1.25% of the monomers were labeled with DR1. With this very small doping amount, we reached an amplification of the dielectric signal by a factor 15 in thick films, which is in line with the results of previous synthesis. For example, dispersion of 1% (w/w) of 4,4'-(N,N-dibutylamino)-(E)-nitrostilbene (DBANS) increased the dielectric strength of PS by a factor of 5 [148,150], while the dielectric loss of PS ( $M_w = 13$  kg/mol) was enhanced 65 times after covalently attaching DR1 (3% w/w) directly onto the backbone. Analysis of the segmental mobility provided that our labeling procedure did not alter the glass transition temperature ( $= 373.4 \pm 1.0$  K), nor the dynamic fragility  $m_p$  ( $= 131 \pm 10$ ). Consequently, the dynamics of the doped chains in contact with neat PS corresponds to the dynamics of l-PS enslaved to its own gradient of mobility, that is, the presence of PS does not alter the relaxation behavior of l-PS. Moreover, upon confinement, ultrathin films of the labeled polymer (l-PS) showed the typical features characterizing the thickness dependence on the  $\alpha$ -process at the nanoscale: shift in  $T_\alpha$  (here towards higher temperatures, which is indicative for a slowing down of the molecular dynamics), increase in the width of the  $\alpha$ -peak and reduction of the dielectric strength [65]. These characteristics made l-PS a perfect candidate to check if those features arise from the distribution of segmental mobility in capped films.

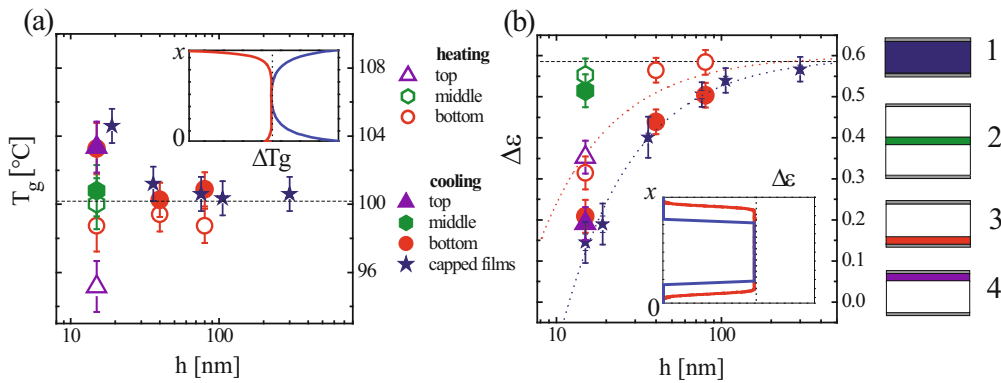


**Fig. 18.** Values of glass transition temperature,  $T_g$ , (a) and dielectric strength,  $\Delta\epsilon$ , (b) are reported for different thickness and sample configurations. Colors of the symbols correspond to the color chosen for the different geometries sketched on the right. Open symbols are used for the values measured in heating and solid symbols for those in cooling. Sketches of the profiles of  $T_g$  (a) and  $\Delta\epsilon$  (b) along the film thickness in heating (red) and in cooling (blue) are given as insets. Reproduced from Rotella *et al.* [11] with permission of the American Chemical Society.

Multilayer films were modeled as a series of capacitances where the total capacitance  $C_{\text{tot}}^*$  is given by  $\frac{1}{C_{\text{tot}}^*} = \frac{1}{C_{\text{labeled PS}}^*} + \frac{1}{C_{\text{neat PS}}^*}$  and  $C_{\text{labeled PS}}^*$  and  $C_{\text{neat PS}}^*$  are the complex capacitance of the layer of l-PS and of the layer of neat PS, respectively. After determining the intrinsic contribution of neat PS, it was possible to extract the contribution of the labeled layer from the total response of the multilayer film. An example of the quality of the data extracted via this procedure is given in fig. 17.

Differently from previous work, we wanted to check if thermal annealing in the liquid state could affect the behavior of chains at the interface and thus the gradients of molecular mobility. For this purpose, we measured the response of multilayer films both during heating (303 K  $\rightarrow$  423 K) and cooling (423 K  $\rightarrow$  303 K) scans performed with an effective scanning rate of 0.3 K/min. These two experimental conditions correspond to, respectively, short and long annealing times. In fact, provided that time-temperature superposition is fulfilled [72], changes in the interfacial properties should scale with the same activation energy as the structural relaxation, *i.e.* annealing at higher temperatures compares to longer annealing times at a lower temperature. This speculation was finally verified by noticing that the changes during annealing follow the adsorption kinetics, that is, have the same activation energy as the structural process, see subsect. 2.5.1. We assembled multilayers composed of 45 nm thick films of PS and 15 nm thick films of l-PS, and mapped the values of the segmental relaxation time and of the dielectric strength at different distances from the polymer/metal interface, see fig. 18.

The value of  $T_g$  and of  $\Delta\epsilon$  of the 15 nm thick layer of l-PS placed between two 45 nm layers of neat PS (geometry 2) exhibits bulk values over the two thermal cycles of heating and cooling. On the contrary, a clear deviation from bulk behavior was found in those multilayers where the l-PS film was placed in direct contact with Al. Moreover, we observed that the relaxation behavior of the interfacial layers was affected by annealing.

In particular, for geometry 3 and 4, that is, when the labeled chains were in contact with the upper or the lower electrode, during the heating scan the dielectric strength of l-PS was reduced to 70% of its bulk value. After reaching 423 K and successive cooling,  $\Delta\epsilon$  dropped further till reaching  $\sim 30\%$  of its value in thicker films. This evidence implies that the number of molecules participating to the structural relaxation in proximity of a metallic interface is smaller than in bulk and that such a number decreases upon further annealing, due to irreversibly chain adsorption. This result could finally disprove that the reduction in dielectric strength observed in thin films is due to a reduced cooperative character of the structural relaxation in interfacial layers [151]. Following our simplified definition, see subsect. 2.2, the dielectric strength can be written as the product of the dipole density number and the square of the dipole moment,  $\Delta\epsilon = \tilde{N}\mu^2$ . If  $n$  neighboring dipoles relax cooperatively, the effective density number drops to  $\sim \tilde{N}/n$  and the dipole moment rises to  $\sim n\mu$ ; under those conditions the dielectric strength scales as  $\Delta\epsilon = n\tilde{N}\mu^2$ . The number of the cooperative units  $n$  at the interfaces gets smaller due to the break in the symmetry, consequently  $\Delta\epsilon_{\text{interface}}/\Delta\epsilon_{\text{bulk}} < 1$ . Such hypothesis however, because it is based on mere size effects, cannot justify a change in  $\Delta\epsilon$  upon annealing in a sample of constant thickness. In fact, the introduction of an interface corresponds to a perturbation in the cooperative dynamics taking place on the time scale of the structural relaxation, that is, 10 s at most in our experiment. Considering that the kinetics of the drop in  $\Delta\epsilon$  occur on much longer time scales ( $\gg \tau_{\text{REP}}$ ), we should reject this hypothesis. Moreover, a smaller cooperativity should always be accompanied by an enhancement in relaxation rate [2], because of the lower hindrance in the molecular motion. On the contrary, while we observed negative values of  $\Delta T_g$  in the heating scan, upon cooling, we detected an increase in  $T_g$ . In particular, concentrating on the upper interface (results for the l-PS layer in contact with the lower electrode are shown in fig. 18 during the heating scan, at bulk  $T_g \tau$  (extrapolated via a VFT fit) decreases by 2 orders

of magnitude, while it exceeded its bulk value by a factor 7, after annealing at 423 K. Same as for  $\Delta\varepsilon$ , the dielectric function is not affected by annealing if the films of l-PS are not in direct contact with Al.

We did not observe any change in the segmental mobility when we placed a thicker layer of l-PS (40 and 80 nm in geometry 3, fig. 18) in contact with the metallic interface. Thus, perturbations on the mobility should decay at a few tens of nm from the bounding interface. However, such a length scale could be underestimated; in fact, because of the drop of  $\Delta\varepsilon$  in the physisorbed layer, the weight of those interfacial chains assuming conformations different from the bulk and generating the perturbation in  $T_g$  [18] is reduced in comparison to bulk-like layers.

Finally, it is worth reminding that the sample preparation of the layers in the two geometries is rather different. The conformations adopted by polymer chains in geometries 3 and 4, immediately after preparation, are intrinsically different. At the lower interface (geometry 3) chains get adsorbed from a dilute solutions onto the surface and suffer quick changes in the viscosity, due to the rapid evaporation of the solvent during spincoating; on the contrary, at the upper electrode (geometry 4), molecules facing a free surface are finally covered by metal atoms thermally evaporated in high vacuum. The asymmetry in the sample preparation is erased upon mild annealing, probably within the time scale of the structural relaxation time, that is, considering our slow scanning rates ( $\sim 0.5$  K/min) differences between the two interfaces disappear fast after curing the multilayers above  $T_g$ .

The experimental evidence collected in this work permitted to justify the use of symmetric profiles in the analysis of the thickness dependence of quantities averaged over the film thickness. In the following sections we provide two examples based on the solution of inverse problems that permitted to obtain profiles in molecular mobility based on the dielectric strength and the thermal expansion.

#### 4.5 Gradients of molecular mobility obtained via the density number of molecules participating to the glass transition

Isothermal experiments in the liquid state revealed a correlation between the drop in dielectric strength and the thickening of the irreversibly adsorbed layer formed onto solid interfaces, see subsect. 2.3 [23]. Due to experimental problems related to the difficulties in preparing very thin freely standing films necessary for the multilayer experiments, at the state of the art it is not possible to map the values assumed by  $\Delta\varepsilon$  with a resolution smaller than 15 nm via the multilayer approach presented in the previous section [11]. In the attempt to reduce this limit, we studied the thickness dependence of the dielectric strength,  $\Delta\varepsilon(h)$ , which permitted obtaining profiles of molecular mobility, based on the number of molecules participating to the glass transition.

As shown in subsect. 2.5, regardless of the change in segmental mobility and the sign of  $\Delta T_g$ , upon confinement,  $\Delta\varepsilon$  gets continuously reduced upon increase of the

surface to volume ratio, see fig. 2 (bottom panel). In analogy to a cold crystallization process, the reduction of this reflects the decrease of the density number of the fluctuating dipoles contributing to the dielectric signal [81, 120, 152]. For various polymer systems, the decay of  $\Delta\varepsilon$  vs.  $h^{-1}$  in isothermal conditions was approximated by a linear trend, which implies a sharp mobility profile at the two interfaces [153–155]

$$\frac{\Delta\varepsilon(x)}{\Delta\varepsilon_{\text{bulk}}} = \begin{cases} 0, & x \leq \delta_L \cup h - \delta_L < x < h, \\ 1, & \delta_L < x < h - \delta_L. \end{cases} \quad (26)$$

In fact, linear fits of the type  $\Delta\varepsilon(h) = \Delta\varepsilon_{\text{bulk}}(1 - 2\delta_L/h)$  reproduce this trend, by means of a step-like Heaviside function consisting of a bulk layer capped between two dead layers (DL) of identical thickness  $\delta_L$ , where  $\Delta\varepsilon = 0$  at each interface. The term “dead” reflects the conjecture that the interfacial regions are composed of adsorbed molecules whose structural relaxation is inhibited at the time scales investigated over the whole experimental temperature range [117]. In the following subsections we will show that this consideration does not apply to all polymers. However, investigation of other systems revealed also the unusual scaling  $\Delta\varepsilon \sim h$  [156], together with several cases where the reduction in the dielectric strength cannot be satisfactorily reproduced by a linear dependence of the type  $1 - \text{const}/h$  [16, 153]. The observed pronounced non-linear reduction of the dielectric strength upon increase of the surface to volume ratio suggests the presence of a strong gradient of molecular mobility along the distance from the metallic interfaces. Therefore, we thought that the incorporation of a continuous distribution of density number of fluctuating dipoles across the film,  $\tilde{N}(x)$ , would bring to a more realistic scenario, including broadening arising from the spatial heterogeneity in the segmental mobility.

With these considerations in mind, we have developed a new model, able to reproduce the thickness dependence of the dielectric strength ranging from the  $\sim h^{-1}$  to the  $\sim h$  decaying behavior and to provide profiles of mobility for all the systems of which the thickness dependence of  $\Delta\varepsilon$  is known [65].

To reproduce the mobility gradient of the density of fluctuating dipoles in proximity of an interface,  $\Delta\varepsilon(x) \sim \Delta\varepsilon^{\text{BULK}} \tilde{N}(x)$ , we readapted a smooth profile derived from a Landau-Ginsburg free energy functional theory [157], developed to describe the density distribution of a polymer melt in contact with solid walls. The analytical equation, in the case of neutral or repulsive wall, that is, a reduction of density at the interface, reads

$$\phi(x) = \phi_b \tanh^2 \left( \frac{x}{2\psi_S} + A \right), \quad (27)$$

where  $\phi_b$  is the bulk density,  $\psi_S$  is the correlation length of the surface profile, and  $A$  is a shift parameter incorporating the boundary conditions. The profile in eq. (27) describes an interfacial layer of lower density, extending for a thickness on the order of  $3 \cdot 2\psi$ , where the bulk value

is recovered, ( $\tanh^2(3) \sim 1$ ). To describe a distribution of  $\Delta\varepsilon$  in capped films, we have adjusted this density profile extending it to the case of a polymer layer capped between two non-repulsive symmetric solid surfaces. Under the assumption of a smooth distribution of segmental mobility, we replaced the density with the dielectric strength. This substitution is licit considering that interfaces contribute to a decrease of  $\Delta\varepsilon$  ( $\Delta\varepsilon_{\text{interface}} < \Delta\varepsilon_{\text{bulk}}$ ) [11]. For capped films, the profile in  $\Delta\varepsilon$  thus reads

$$\Delta\varepsilon(x) = \Delta\varepsilon^{\text{bulk}} \left[ \tanh^2 \left( 3 \frac{x}{\varphi} + \rho \right) + \tanh^2 \left( 3 \frac{h-x}{\varphi} + \rho \right) - \tanh^2 \left( 3 \frac{h}{\varphi} + \rho \right) \right], \quad (28)$$

where  $\varphi$  is here the penetration depth of the interfacial reduction in dielectric strength and  $\rho$  is the shift parameter, *i.e.* the value of  $\Delta\varepsilon$  at the very interface is reduced to a fraction corresponding to  $\tanh^2(\rho) = \Delta\varepsilon_{\text{interface}}/\Delta\varepsilon_{\text{bulk}}$ . The advantage of eq. (28) is the straightforward determination of two fitting parameters  $\varphi$  and  $\rho$  related to material properties.

To obtain the best fitting parameter for each data set (*i.e.* the values of  $\Delta\varepsilon(h)$  at constant  $T$ ), the experimental data were compared to values calculated averaging the gradient in eq. (28). This procedure required the calculation of the total dielectric response of a film of thickness  $h$ , via a layer-resolved approach, whose validity is supported by previous simulation work on the dielectric relaxation at the nanoscale. In our computation, the film was divided into  $h$  sub-layers, and attributed to each of those a dielectric function reproduced by the an HN equation, see eq. (7), where the position and the shape of the peak of each sublayer is kept constant and the dielectric strength is varied, following a profile given by discretization in steps of 1 nm of eq. (28). Because in the capped geometry the orientation of the electric field is perpendicular to the polymer/metal interface, the total dielectric response was obtained summing up the contributions of each sub-layer, as for capacitors in series,  $C_{\text{TOT}}^{-1}(f, T) = \sum_j C_j^{-1}(f, T)$  where  $C_j(f, T)$  is the capacitance of the  $j$ -th sub-layer. To reduce errors introduced by numerical integration, the value of  $\Delta\varepsilon_{\text{TOT}}$  was obtained directly from the real part of the computed dielectric function following its definition, as the difference between  $\varepsilon_S$ , the frequency-independent value reached by the real part of the dielectric function for  $\omega \ll \omega_0$ , and  $\varepsilon_\infty$ . We considered a frequency range broad enough to take into account the broadening of the structural peak, *i.e.* a larger separation between the frequency regions corresponding to  $\varepsilon_S$  and  $\varepsilon_\infty$ , and the shift in the peak maximum upon confinement. The assumption that the shape parameter and the peak position do not influence the value of  $\Delta\varepsilon$  is justified by the evidence that, in ultrathin films of amorphous polymers, the dielectric strength depends only the interaction with the substrate and on the annealing conditions [23].

As it was not possible to solve the problem analytically, we extended the procedure to a matrix of couples  $(\varphi^i, \rho^i)$  centered around physically reasonable starting parameters, and found the best fitting values for the experimental values, upon minimization of the squared deviations:

$$\text{Err} = \frac{1}{n_{\text{exp}}} \sum_{i=1}^{n_{\text{exp}}} \left( \frac{\Delta\varepsilon_i^{\text{th}} - \Delta\varepsilon_i^{\text{exp}}}{\Delta\varepsilon_i^{\text{exp}}} \right)^2,$$

where  $n_{\text{exp}}$  is the number of the experimental data points, that is, the number of thicknesses measured at each temperature,  $\Delta\varepsilon^{\text{th}}$  and  $\Delta\varepsilon^{\text{exp}}$  are, respectively, the values of the dielectric strength obtained via our model and experimentally.

In addition to the numeric approach, we obtained an approximated solution of the inverse problem related to the thickness dependence of the dielectric strength, considering the special case of zero residual polarization at the interface, and neglecting the effects of the direction of the electric field. Under these assumptions, applying the mean value theorem, we obtained the expression

$$\frac{\Delta\varepsilon(h)}{\Delta\varepsilon_{\text{bulk}}} = 1 - \frac{\tanh(h/\varphi)}{h/\varphi}, \quad (29)$$

which satisfactorily reproduces the experimental trends and numerically values for the drop of  $\Delta\varepsilon$ . In particular, eq. (29) shows that if the condition  $h/\varphi \gg 1$  is satisfied,  $\Delta\varepsilon$  scales linearly with the surface to volume ratio,  $\Delta\varepsilon(h)/\Delta\varepsilon_{\text{bulk}} \sim 1 - \text{const}/h$ ; this is possible for films much thicker than the penetration depth of the dielectric strength. On the contrary, at large values of  $\varphi$ , *i.e.* when  $h/\varphi \ll 1$ , the right side of eq. (29) becomes  $\sim 1 - h/\text{const}$ , which reproduces the exotic behavior reported for hyper-branched polyesters. This trend is justified by the complex tridimensional molecular structure of this polymer, characterized by longer length scales than those of homopolymers. Thus  $\varphi$  can be seen as a broadening parameter sensitive to the different chain architectures, and its increase sets the transition from a sharp mobility profile to a broader distribution of  $\Delta\varepsilon$ .

Regardless of the value of  $\varphi$ , in proximity of  $\varphi^{-1}$ ,  $\Delta\varepsilon$  vs.  $h^{-1}$  shows a bending, indicating that the drop in the thickness dependence of  $\Delta\varepsilon(h)$  slows down. Examples of the fits are reported in fig. 19, while the corresponding mobility profiles are indicated in fig. 20, where, for the sake of simplicity, we considered films thick enough to avoid the reciprocal influence of the two interfaces ( $h \gg 2\varphi$ ).

For all the polymers investigated, three different zones characterize the form of the gradient of mobility obtained from the dielectric strength. In the *first zone*, extending for a couple of millimeters (except in the exceptional case of hyper-branched polyesters, where this layer occupies almost 20 nm),  $\Delta\varepsilon$  is constant. Depending on the positive or null values adopted by  $\Delta\varepsilon$  in this region, we divided the investigated systems in two groups. If  $\Delta\varepsilon$  reaches negligible values in proximity of the metallic surface, then  $\rho = 0$  and a dead layer is formed; the values obtained by our computation are in line with those estimated by ellipsometry. When  $\rho > 0$  we reproduced the behavior of

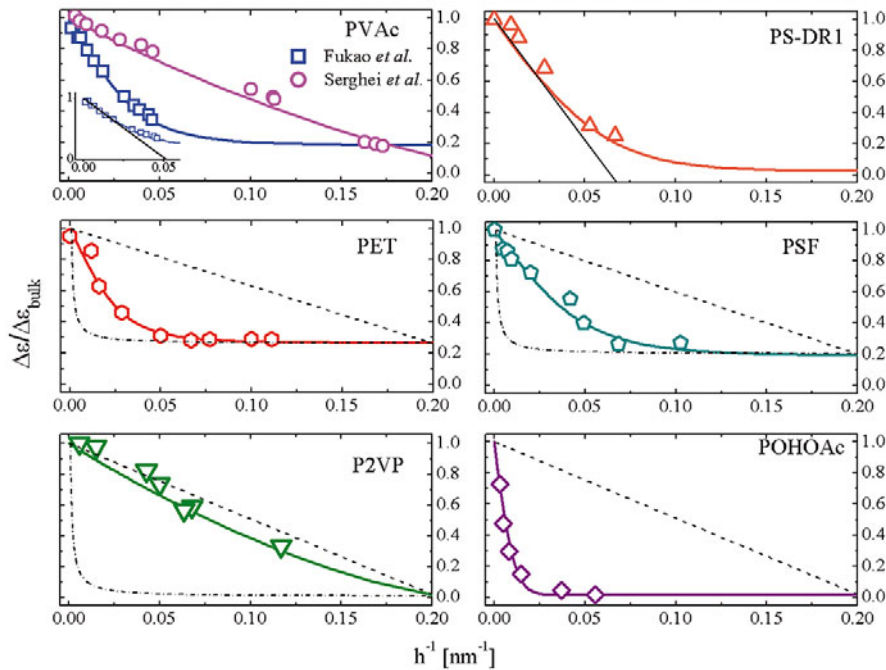


**Fig. 19.** Normalized dielectric strength *vs.* inverse of the film thickness for the polymers listed in fig. 2 (lower panel). The continuous curves are fits of the experimental values, obtained from averaging eq. (28) via the procedure described in the text. The dashed and the dotted-dashed lines represent respectively the  $\sim -h^{-1}$  and the  $\sim h$  drops of the dielectric strength. The inset shows the deviation of the experimental and calculated trends for samples of PVAc from linear fits,  $1 - \text{const}/h$ . Reproduced from Rotella *et al.* [65] with permission of the Royal Chemical Society.

a reduced mobility layer, where a non-zero residual polarization is present near the wall. We noticed that the presence of such a residual degree of mobility inside the first interfacial layer is in agreement with the prediction of the TOP model, where the BOO increases in proximity of the wall, due to larger interparticle correlations, that is larger  $g$  [39]. We experimentally validated this trend in the case of glycerol, where in proximity of a quartz substrate, the dielectric strength was twice as large as in bulk [57].

A *second zone*, covering length scales  $\sim \varphi$  (10–100 nm), separates the dead or reduced mobility layer from the bulk core of the film, where  $\Delta\varepsilon/\Delta\varepsilon^{\text{BULK}}$  is 1. It is worth mentioning that the penetration depths of the drop in  $\Delta\varepsilon$  are comparable to the critical thicknesses where other techniques reported the onset of the deviation from bulk behavior. Thus, we should consider the dielectric strength and not the shift in the relaxation time as the real parameter reflecting the effects of confinement on the dielectric function.

#### 4.6 Profile of thermal expansion via capacitive dilatometry

In this section we describe an example of the use of capacitive dilatometry (CD), a technique exploiting the temperature dependence of the capacitance as a probe of thermal expansion in capped polymer films. Bauer *et al.* introduced a method based on the changes in the high-

frequency response of glass-forming systems during temperature scans [158]. Such a procedure was successively extended to the investigation of thin polymer films by Fukao *et al.* [15], who considered that the temperature dependence of the capacitance is exclusively driven by the expansion coefficient in the normal direction to the surface,  $\alpha_n$ . In fact, in the absence of molecular relaxation processes, the real part of the complex capacitance is directly proportional to the inverse of the distance between the electrode, that is, the film thickness. In case of thin films, the interfacial area  $S$  is constant, and  $\alpha_n$  is given by  $-\kappa \cdot C(T)/C_0$ , where  $\kappa$  is a temperature-independent parameter and  $C_0 = \varepsilon_0 \varepsilon_r S h^{-1}$  is the geometrical capacitance at a chosen reference temperature. Because it senses thermal expansion, this method can be used to assign the glass transition temperature as the crossover between two different linear regimes, whose slopes are proportional to the thermal expansion in the glassy and in the liquid state. Consequently each temperature scan provides three independent parameters:  $\alpha_G$ , the normal thermal expansion coefficient for  $T < T_g$ ,  $\alpha_M$ , the normal thermal expansion coefficient in the liquid state, and  $T_g$ . Differently from ellipsometry, CD offers the possibility to investigate capped films, which by mimicking the properties of model nanocomposites are a benchmark for the investigation of hybrid materials containing organic/inorganic interfaces. Optical techniques encounter large experimental problems on metal/polymer multilayers, due to lack of a direct access on the polymer layer, the large adsorption coefficient

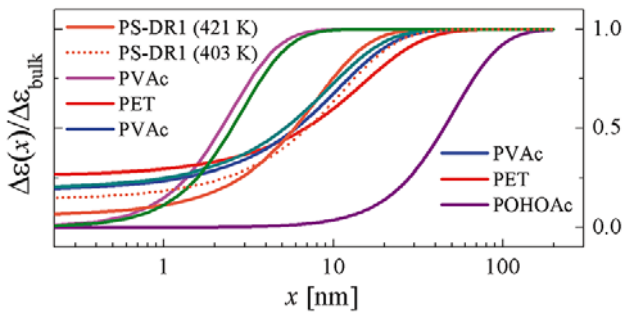


**Fig. 20.** Mobility profiles at one interface for thick samples of various polymers, continuous curves were obtained from eq. (28) using the corresponding best fit values of  $\phi$  and  $\rho$ . Reproduced from Rotella *et al.* [65] with permission of the Royal Chemical Society.

of the metallic coatings, and the scattering of light onto rough surfaces; on the contrary, CD does not “see” the conductive layer, and thus it senses only the dielectric medium, *i.e.* the polymer.

#### 4.6.1 Dead layers

In the case of capped films, where two buried interfaces are present, we can expect a behavior similar to that seen for the dielectric strength. Chain pinning onto the metallic interface, in fact, reduces the thermal expansion of interfacial layers, yielding to the formation of dead layers, DL, where thermal expansion is virtually zero. The existence of such a layer was furthermore confirmed by Gin *et al.*, who showed lack of temperature dependence in the thickness of an irreversibly adsorbed layer of PS, grown under equilibrium conditions [80] ( $t^* \gg 1$ , see subsect. 2.4). Although having a large affinity, “dead layers” and “adsorbed layers” should not, however, be confused; in the latter case a non-zero thermal expansion could be present (see the case of PTBS discussed below). Finally it is noteworthy that the measured value of  $\delta_L$  depends on the experimental approach used [159]: methods sensing localized segmental motions (rotations, vibrations of the different chemical groups) probe shorter immobilized layers in comparison to techniques averaging over larger angular fluctuations. Based on these simple considerations, we proposed a symmetric model for CD, where a bulk like layer is embedded into two dead layers of constant thickness [117]

$$\begin{cases} \alpha_G(h) = \left(1 - \frac{2\delta_L}{h}\right) \alpha_G^\infty, & T < T_g, \\ \alpha_M(h) = \left(1 - \frac{2\delta_L}{h}\right) \alpha_M^\infty, & T > T_g. \end{cases} \quad (30)$$

The upper index “ $\infty$ ” indicates the value of a very thick sample. The validity of this model is tested by fitting the experimental data collected for ultrathin films of PS160 capped between Al layers, annealed for 12 h at  $T_g + 25$  K. For this system, we observed higher  $T_g$ 's in the thinner films ( $\Delta T_g = 15$  K at 7 nm) and obtained

$\delta_L = 2.7 \pm 0.4$  nm, in line with the values estimated by ellipsometry [13,137] and our approach on the thickness dependence of  $\Delta\varepsilon$ , see subsect. 4.5.

Surprisingly, in this case it was not necessary to add a correction for broadening, in fact, the drop in thermal expansion (both above and below  $T_g$ ) was linear with the inverse of the thickness down to at least 7 nm, *i.e.* if different than 0, the value of  $\varphi$  is limited to  $3.5$  nm  $\sim \delta_L$ . The corresponding thermal expansion profile is thus given by a very sharp function, in line with observations in other similar investigations by means of ellipsometry [14].

Measurements in samples thinner than  $2\delta_L$  revealed a completely different scenario. In this case the capacitance increased upon heating, implying a negative thermal expansion coefficient. Considering the reversible character of this phenomenon, we proposed a mechanism of “defreezing” of the dead layer, similar to the melting of the rigid amorphous fraction in semicrystalline systems, which causes an increase in local free volume [117]. The larger electric capacitance at higher temperatures is due to an orientational (dipolar) polarization process related to partial desorption of the immobilized chains. Recently, Koga and coworkers demonstrated that the activation energy of this process corresponds to changes in the local conformations of the chain, and that the densification (less free volume) occurring in the adsorbed layer upon cooling is due to the enrichment in *trans* states, or better a reduction in *gauche* states, corresponding to more flattened (less mobile) chains [80].

#### 4.6.2 The unusual case of PTBS: Where adsorption speeds up the dynamics

The investigation of the thickness dependence of the thermal expansion of capped films of poly(4-tertbutyl styrene), PTBS, revealed a more complex and highly unusual scenario [19]. PTBS is a polystyrene derivate, where the 4-(para) position of the aromatic ring is replaced by the bulky apolar tertbutyl group. The interest in this system arose from the report of the largest onset in the effect of confinement (400 nm *vs.* the typical 20–100 nm), as indicated by fluorescence spectroscopy ( $\Delta T_g = -50$  K at 25 nm) [160], and alternative approaches based on the efficiency of polymer/pentacene transistors [161].

By means of CD, we observed a modest reduction in the transition temperature ( $\Delta T_g \sim -8$  K, for 7 nm) and a drop of both the thermal expansion coefficients ( $\alpha_M \sim 0.15 \alpha_M^\infty$  and  $\alpha_G \sim 0.20 \alpha_G^\infty$ , at 7 nm). Remarkably, the drop in  $\alpha_{M,G}$  did not scale linearly with the inverse of the thickness, see fig. 21. The combination of these results might seem contradictory: we observed an enhancement of the structural dynamics ( $\Delta T_g < 0$ ) coupled to a reduction of thermal expansion.

The apparent paradox was solved considering the unusual non-linear change of the thermal expansion coefficients with  $h^{-1}$ . Showing a concave profile, such a trend could not be explained in terms of interfacial broadening, which on the contrary provides the opposite convexity as for  $\Delta\varepsilon(h^{-1})$ , see subsect. 4.5. We noticed that, below a

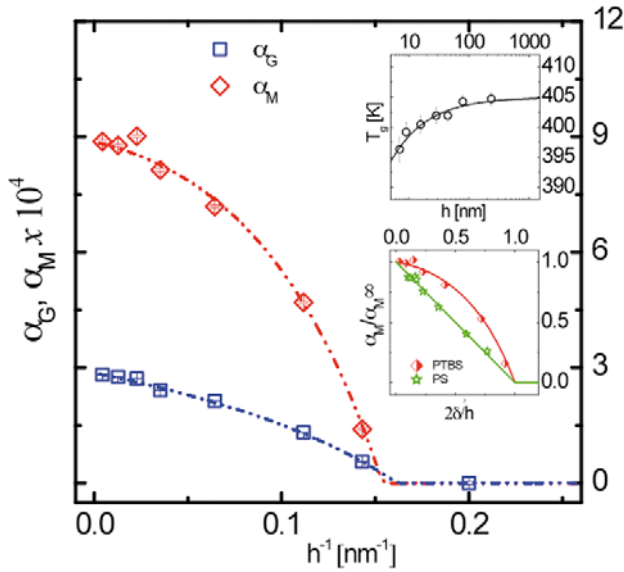


**Fig. 21.** Thermal expansion coefficients of ultrathin films of PTBS, as a function of the inverse of the thickness. The dash-dotted lines are fit to the experimental data via eq. (3). In the upper inset, thickness dependence of the glass transition temperature, the line follows the equation  $T_g(h) = 405 \cdot (1 - (0.13/h)^{0.6})$  K. In the lower inset, the thickness dependence of the thermal expansion coefficient in the melt for films of PTBS (red diamonds) and PS (green stars) prepared in similar annealing conditions, see text. To facilitate comparison, data were normalized to the bulk value of the thermal expansion coefficient and to the total extension of the dead layer. Reproduced from Napolitano *et al.* [19] with permission of the American Chemical Society.

critical thickness, same as for PS, we could not detect a positive thermal expansion, and that we could adequately fit our results via an interpolation with a quadratic function in  $h^{-1}$ . Consequently we thought of a symmetric thermal expansion profile  $L(x)$  of the form

$$L_\alpha(x) = \begin{cases} 0, & 0 < x < \delta_{G,M} \cup h - \delta_{G,M} < x < h, \\ \alpha_{G,M}^\infty \left( 1 + \frac{\lambda_{G,M}^2}{x^2} + \frac{\lambda_{G,M}^2}{(h-x)^2} \right), & \delta_{G,M} < x < h - \delta_{G,M}, \end{cases} \quad (31)$$

which upon solution of the related inverse problem brought to the following expression of the thermal expansion coefficients:

$$\frac{\langle \alpha(h) \rangle_{G,M}}{\alpha_{G,M}^\infty} = \begin{cases} 0, & h < \delta_{G,M}, \\ 1 - 2 \left( \delta_{G,M} - \frac{\lambda_{G,M}^2}{\delta_{G,M}} \right) \frac{1}{h}, & \delta_{G,M} < h < h + \delta_{G,M}, \\ -2 \frac{\lambda_{G,M}^2}{h(h - \delta_{G,M})}, & h \geq h + \delta_{G,M}. \end{cases} \quad (32)$$

Equation (32) is the superposition of two Heaviside functions (dotted line) and two power law branches, (dash

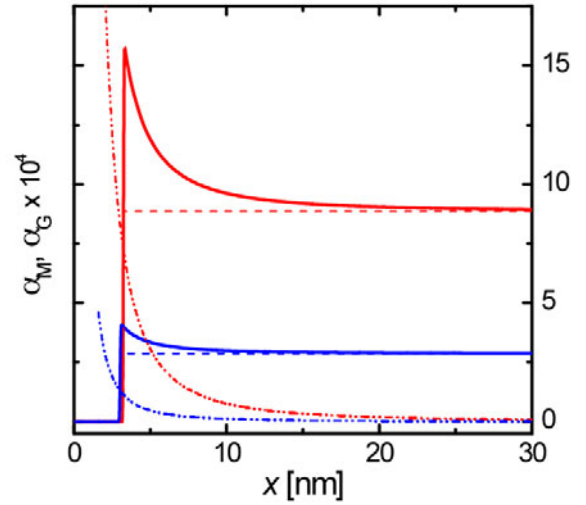


**Fig. 22.** Reconstructed profile of the thermal expansion in the melt (red) and in the glass (blue), referring to the data plotted in fig. 21. Single contributions from the Heaviside step due to the dead layer (dashed line) and to the decay of interfacial conformation correlation function (dash-double-dotted line) are also given. Only half of the profile is plotted, being this symmetric with respect to the middle of the film. Reproduced from Napolitano *et al.* [19] with permission of the American Chemical Society.

dotted lines) bound to the parameters  $\lambda_{G,M}$ , symmetric towards the core of the film. For the melt we find  $\delta_G = 3.1 \pm 0.5$ ,  $\lambda_G = 2.0 \pm 0.2$  and  $\delta_M = 3.2 \pm 0.5$ ,  $\lambda_M = 3.0 \pm 0.2$ ; all values are expressed in nm. The analytical form of  $L_\alpha(x)$  provided a clear physical picture for the increase of the thermal expansion, see fig. 22. The excess in thermal expansion is localized at the interface between the bulk core and the immobilized layer. The non-monotonous character of the gradient is given by the superposition of two competing effects, arising from the reorganization of interfacial chains at different distances from the interface.

At short scales ( $x < \delta_{G,M}$ ), the monomer density exceeds the bulk value due to pinning onto the metallic surface. Consequently segmental fluctuations ensuring large-scale reorientations are highly hindered and thermal expansion assumes values much smaller than in bulk. At longer distances ( $x > \delta_L$ ), instead, the density ( $\sim 1/\alpha$ ) drops quadratically with the distance from the wall due to packing frustration. Remarkably, our experimental data are in line with the scaling expected by mean-field theory for polymers melts in the presence of weakly interacting media [157],  $\sim (\lambda_{G,M}/x)^{-2}$ . Under this framework, we can associate  $\lambda_{G,M}$  to the double of the correlation length for the concentration fluctuations. This quantity grows upon chain stiffening, and is also affected by molecular mobility, *e.g.*  $\lambda_{G,M}$  increases in the liquid state, due to larger interference of rotational motion on packing frustration.

We speculate on the universality of such dual behavior at the polymer/solid interface, and on the possibility to

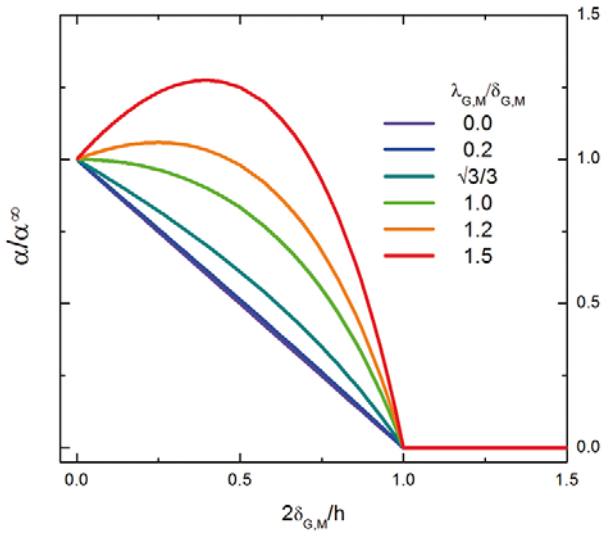


**Fig. 23.** Impact of the ratio between the length scale of the packing frustration and the thickness of the dead layer on the thickness dependence of the thermal expansion coefficient, computed from eq. (32).

tune it by changing the polymer/substrate affinity. In particular, we expect that larger affinities or a higher adsorption degree (larger  $t^*$ ) could be expressed by high  $\delta/\lambda_{G,M}$  ratios. For PTBS, where  $\delta/\lambda_{G,M} \sim 1$ , it was possible to fit the thickness of the thermal expansion via eq. (32). Increasing the value of  $\delta/\lambda_{G,M}$ , the non-linear character of  $\langle \alpha(h^{-1}) \rangle_{G,M}$  decreases and it becomes more difficult to detect the presence of the excess in thermal expansion, that is, a linear trend of  $\alpha_{G,M}$  vs.  $h^{-1}$  is recovered. Considering reasonable standard deviations on the experimental data, such a condition is reached in proximity of the threshold  $\delta/\lambda_{G,M} > \sqrt{3}$ . On the contrary, when  $\delta/\lambda_{G,M} < 1$ , a clear maximum appears at thicknesses on the order of  $4\delta$ , see fig. 23. This situation reflects the minimum in density found for nanocomposites of polyhedral oligomeric phenethylsilsesqui-oxanes (POSS) dispersed in a matrix of PC with a low content of the inorganic phase [162]. Remarkably, dispersion of the same filler in PS, where the aromatic moieties increase the affinity with POSS and thus  $\delta/\lambda_{G,M}$ , yielded a full recovery of the linear trend of the density with the nanoparticle concentration (scaling as  $h^{-1}$ ), as expected.

## 5 Conclusions and open questions

In this Colloquium we discussed on the large experimental evidence collected in the last years on the impact of packing frustration and irreversibly chain adsorption on the dynamics of ultrathin polymer films. In particular, we showed a striking correlation between the kinetics of adsorption and the evolution of the glass transition temperature upon prolonged annealing in the liquid state. We discussed on the non-equilibrium character of polymer films upon nanoscopic confinement, arising from the fast

evaporation of solvent during spincoating and the sluggish character of the kinetics of irreversible chain adsorption. Consequently, we argued that criteria of “equilibration” holding in the case of entangled bulk melts, as for example thermal annealing at times exceeding the reptation time, are not valid upon confinement. On the contrary, we verified that the shift in  $T_g$  is proportional to the thickness of the layer irreversibly adsorbed during annealing in the liquid state and proposed a new “equilibration” criterion based on the dimensionless number  $t^*$ , defined by the ratio between the annealing time and the time scale of adsorption. At  $t^* > 1$ , the kinetics of chain adsorption slows down and the correlated changes in the glassy dynamics are negligible in comparison to the largest perturbations at shorter annealing times. Consequently, we propose that at  $t^* > 1$  a new steady state (with a lifetime exceeding the time scales of technological interest) is reached. We anticipate that the structure of films prepared at  $t^* \sim 1$  scales as expected for the reflected random walk of an equilibrium melt immobilized by the surface ( $h \sim N^{1/2}$ ), which further validates our hypothesis [163].

We highlighted a direct proportionality between the shift in  $T_g$  and the thickness of the Guiselin brush (irreversible adsorbed layer) at constant  $t^*$ . To understand the molecular origin of this correlation, we developed a molding approach, which, at the state of the art, is the only method permitting to determine the variations in interfacial free volume in ultrathin polymer films. The molding experiment finally confirmed that the interfacial free volume is directly proportional to the shift in  $T_g$  upon confinement. Consequently, we verified that packing frustration (excess in free volume) is a source of faster dynamics, which induces a reduction in  $T_g$  in proximity of the polymer/solid interface, even in the presence of chain adsorption.

In this Colloquium, we have also described different experimental methodologies, through which it is possible to investigate by means of dielectric spectroscopy the dynamics of polymers and low-molecular-weight glass-formers in capped, supported and freely standing films, that is, respectively without, with one, and with two free surfaces. We proposed several examples of the solution of inverse problems related to data collected in the above-mentioned methodologies, which allowed the determination of profiles of molecular mobility and thermal expansion in a large number of molecules.

We stressed on the unexploited potentiality of the dielectric strength,  $\Delta\varepsilon$ , the contribution of orientational polarization to the glassy dynamics. We showed that  $\Delta\varepsilon$  is particularly sensitive to the number density of molecules relaxing on the time- and at the length-scale of the dynamic glass transition, and can thus be used to monitor immobilization. The reduction in orientational polarization upon irreversible chain adsorption introduces a gradient of  $\Delta\varepsilon$ , which affects the dielectric relaxation of polymers under confinement, and its interpretation. Due to the lower values assumed by  $\Delta\varepsilon$  near a metallic wall, the largest contributions to the measured signal come from the chains in the middle of the film. As a consequence,  $\Delta\varepsilon$  is affected by confinement already at hun-

dreds of nanometers while the relaxation time, linked to dynamic properties, either remains constant or varies at much higher surface/volume ratios. In fact,  $\tau$  is not an additive quantity, because it is given by the superposition of the modes involved in the molecular process. In the specific case of dielectric spectroscopy, the contribution of the relaxation modes associated to the different sub-layer is not weighted over its volume percentage (due to both the series-model sum required for the dielectric functions and the asymmetric broadening of the  $\alpha$ -peak). The non-linear character of these effects yields an effective reduction of the impact of nanoscopic confinement on  $\tau$ . Consequently, investigation of confinement effects in ultrathin films cannot be limited to the apparent (lack of) changes of the relaxation time and thus of the glass transition temperature.

We conclude this Colloquium with a list of open questions on the dynamics of soft matter under confinement, which we hope will stimulate further investigation and discussion.

1) *How can a gradient of mobility propagate for length scales exceeding the molecular size? What is the molecular mechanism behind the transmission of the confinement effects? How is it possible to enslave the dynamics of a layer to its surroundings?*

The determination of profiles of molecular mobility via the thickness dependence of averaged quantities revealed that the changes in chain conformations run for several tens, sometimes hundreds, of nanometers. de Gennes proposed a “sliding motion” where kinks diffuse along loops acting as vectors of free volume from the polymer/air interface towards the core of the film [89]. Multilayer experiments showed that this mechanism is not sufficient to explain the shift in  $T_g$  in freely standing films [144]. Local measurement of the viscosity showed that the presence of an irreversibly adsorbed layer in the “equilibrium” regime,  $t^* \gg 1$ , affects the properties of the free surface up to distances on the order of  $5-6R_g$  [131]. Could we explain these extreme length scales in terms of rearrangements in the chain conformations upon irreversible chain adsorption?

2) *Why low-molecular-weight glass formers exhibit smaller deviations from bulk behavior?*

The higher conformational entropy introduced by monomer connectivity tremendously increases the possibility to perturb molecular conformations upon confinement. Consequently, correlating deviations from bulk behavior to the stability of interfacial conformations, polymers should show larger shifts in the transition temperatures. However, at low connectivity a different phase can be more stable in proximity of a solid interface. Should we consider the broad region within the full breath of the interfacial mobility gradient as a thermodynamically stable phase different from the bulk?

3) *What is the impact of interparticle correlations on the liquid dynamics? Can we think of the free volume in terms*

*of a reduction in interparticle correlations? Are free volume, packing frustration and bond orientational order correlated?*

The two-order-parameter model predicts an increase in the correlation among the particles of a liquid in proximity of a solid interface, not requiring a change in density. Slower interfacial dynamics should arise from the larger orientational order near the wall [39]. We verified the validity of this idea in the case of the low-molecular-weight glass-former glycerol [57]; what about polymers? How does connectivity influence this structure/dynamics interplay? This criterion for an increase in  $T_g$  is similar to the correlation found between the reduction in  $T_g$  and the increase in interfacial free volume [18].

4) *Is it possible to predict the time scales of re-entanglement and irreversible chain adsorption? Does confinement affect these processes?*

The equilibration of thin films prepared by spincoating requires times much longer than the reptation time. Experiments performed on freeze-dried bulk samples verified that the time necessary to reconstruct the entanglement networks exceeds by several orders of magnitude the reptation time of disentanglement. A solid theoretical framework capable to quantify the separation between these two time scales, and the molecular mechanism of re-entanglement is missing [109]. The comprehension of this phenomenon and a deeper analysis of the adsorption of polymer melts (which at the moment is limited to dilute solutions) will help to quantify the time necessary to “equilibrate” polymers under nanoscopic confinement.

5) *Is it possible to observe multiple distinct glass transitions in the same confinement geometry?*

Recent experiments on freely standing films of PS revealed two well-distinct transitions in the thickness dependence of the thickness, following different molecular weight dependences [164]. It is not clear what is the thermodynamic state of the film at temperatures between the two transitions. Could we treat those films as in the case of immiscible blends, exhibiting independent relaxation phenomena, or should we consider the mutual enslaving in the two processes? The answer to these questions will probably permit to reveal the molecular nature of the two transitions.

Bios.

The authors are indebted to Michael Wübbenhorst (KULeuven) for introducing them to the dynamics of soft matter under confinement. SN acknowledges Günter Reiter (Universität Freiburg) for long and stimulating discussions on the impact of non-equilibrium on the dynamics, Gi Xue (Nanjing University), Nicholas Tito, Ronald White and Jane Lipson (Dartmouth College), Daniele Cangialosi (CSIC-UPV/EHU), Emmanouil Glynos (University of Michigan), Polycarpos Pissis (NT University of Athens) and Andreas Schönhals (BAM) for fruitful conversations on free volume and packing frustration.

## List of symbols and acronyms

1D	1-dimensional
$\alpha_G$	normal thermal expansion coefficient
$\alpha_M$	thermal expansion coefficient in the liquid state
$\alpha_n$	expansion coefficient in the normal direction to the surface
$\gamma_{PS}$	polymer/substrate interfacial energy
$\delta$	phase lag
$\delta_L$	thickness of the dead layer
$\Delta\varepsilon$	dielectric strength
$\Delta(h, t)$	confinement energy
$\Delta f(t)$	cantilever resonant frequency
$\varepsilon$ or $\varepsilon^*$	(complex) permittivity
$\varepsilon'$	dielectric constant
$\varepsilon''$	dielectric loss
$\varepsilon_0$	vacuum permittivity
$\varepsilon_\infty$	dielectric constant in the absence of polarization processes
$\varepsilon_r$	medium permittivity
$\varepsilon_S$	static permittivity (real part of the dielectric function for $w \ll w_0$ , frequency independent)
$\zeta$	interfacial free volume
$\eta$	shear viscosity
$\lambda$	length scale necessary to cancel out surface effects
$\Lambda$	low decay rate and the drop in dielectric strength
$\lambda_{G,M}$	length scale of packing frustration in the glassy state and in the melt
$\mu$	dipole moment
$\xi$	length scale of the glass transition
$\Pi$	linear growth rate of thickness of the irreversibly adsorbed layer
$\rho$	residual interfacial polarization
$\sigma$	surface coverage
$\Sigma$	high decay rate and the drop in dielectric strength
$\sigma_C$	conductivity
$\tau$	structural (or segmental) time
$\tau_\infty$	high-temperature limit of the relaxation time
$\tau_g$	relaxation time at $T_g$
$\tau_{HN}$	Havriliak-Negami relaxation time
$\tau_R$	relaxation time
$\tau_{REP}$	reptation time
$\varphi$	penetration depth of the reduction of the dielectric strength
$\phi_b$	bulk density
$\Phi$	full width at half-maximum of the structural peak in bulk
$\psi$	probability function for a conformational state
$\psi_S$	correlation length of the surface profile
$\omega$	angular frequency
$a$	broadening parameter of the HN function
AFM	atomic force microscopy
Al	aluminum
$b$	asymmetry parameter of the HN function
$B$	fragility-related parameter of the VFT equation
BDS	broadband dielectric spectroscopy
BOO	bond orientational order
$C$	capacitance
$C_0$	capacitance empty capacitor
$C_\infty$	electric capacitance in the absence of polarization contributions
CD	capacitive dilatometry
CRR	cooperative rearranging region
$D$	IDE height
DBANS	4,4'-(N,N-dibutylamino)-(E)-nitrostilbene
$D_C$	diffusion coefficient of the conformational states
DL	dead layer
DR1	disperse red one

$E$	electric field
$E_a$	activation energy
EFM	electric force microscopy
EML	enhanced mobility layer
$f$	frequency
FDT	fluctuation-dissipation theorem
FSF	freely standing film
FWHM	full width at half-maximum
$g$	Kirkwood factor
$G_\infty$	instantaneous shear modulus
GSO	glassy structural order
$h$	thickness
$h_{\text{ads}}$	adsorbed layer thickness
$h_{\text{ads}}^{\text{max}}$	saturation value of $h_{\text{ads}}$ after long annealing time
HN	Havriliak-Negami
IDE	interdigitated (comb) electrodes
$J_0$	zeroth Bessel function
$k_B$	Boltzmann constant
$L_\alpha(x)$	mobility profile based on the thermal expansion
LDS	local dielectric spectroscopy
l-PS	polystyrene labeled with 4-[(4-cyanophenyl) diazenyl] phenyl}(methyl)amino
$m$	low-frequency slope of the structural peak in a log-log plot
$m_p$	dynamic fragility
MRCO	medium-range crystalline order
$M_w$	weight-averaged molecular weight
$n$	high-frequency slope of the structural peak in a log-log plot
$N$	polymerization degree
$\tilde{N}$	density number of dipole moments
OTS	octadecyltrichlorosilane
$P$	polarization
P2VP	poly(2-vinyl pyridine)
PC	polycarbonate
PEL	potential energy landscape
PET	poly(ethylene terephthalate)
PHB	poly(3-hydroxybutyrate)
PMMA	poly(methyl methacrylate)
POHOAc	hyperbranched polyester
POSS	polyhedral oligomeric phenethylsilsesquioxanes
PS	polystyrene
PSDR1	polystyrene labeled with disperse red 1
PSF	polysulphone
PTBS	poly(4-t-butylstyrene)
PVAc	polyvinyl acetate
$R$	resistance
RFOT	random first-order transition theory
$R_g$	radius of gyration
RML	reduced mobility layer
$s$	IDE spacing
$T_0$	Vogel temperature
$t^*$	ratio between the annealing time and the adsorption (or crossover) time
$T_\alpha$	temperature of the maximum of the relaxation peak in isochronal conditions
$t_{\text{ads}}$	adsorption time
$t_{\text{ANN}}$	annealing time
$t_{\text{cross}}$	crossover time
$t_{\text{eq}}$	equilibration time
$T_g$	glass transition temperature
TOP	two-order-parameter model
VFT	Vogel-Fulcher-Tammann
$v$	linear growth rate of the thickness of the irreversibly adsorbed layer
$V$	voltage
$V_m$	volume

## References

1. M. Alcoutlabi, G.B. McKenna, *J. Phys.: Condens. Matter* **17**, R461 (2005).
2. G. Adam, J.H. Gibbs, *J. Chem. Phys.* **43**, 139 (1965).
3. V. Lubchenko, P.G. Wolynes, in *Annual Review of Physical Chemistry* Vol. **58** (Annual Reviews, Palo Alto, 2007) pp. 235.
4. H. Shintani, H. Tanaka, *Nat. Phys.* **2**, 200 (2006).
5. H. Tanaka, T. Kawasaki, H. Shintani, K. Watanabe, *Nat. Mater.* **9**, 324 (2010).
6. H. Tanaka, *Eur. Phys. J. E* **35**, 113 (2012).
7. Differently from the RFOT theory, where the formation of the droplets is driven by configurational entropy alone, the TOP model predicts that the formation of MRCOs is induced by two simultaneous processes: the maximization of the density of the system and the maximization concentration of intermolecular bonds.
8. J.A. Forrest, J. Mattsson, *Phys. Rev. E* **61**, R53 (2000).
9. X. Zheng, M.H. Rafailovich, J. Sokolov, Y. Strzhemechny, S.A. Schwarz, B.B. Sauer, M. Rubinstein, *Phys. Rev. Lett.* **79**, 241 (1997).
10. C.J. Ellison, J.M. Torkelson, *Nat. Mater.* **2**, 695 (2003).
11. C. Rotella, S. Napolitano, L. De Cremer, G. Koekelberghs, M. Wübbenhorst, *Macromolecules* **43**, 8686 (2010).
12. R.D. Priestley, C.J. Ellison, L.J. Broadbelt, J.M. Torkelson, *Science* **309**, 456 (2005).
13. E. Donth, *The Glass Transition, Relaxation Dynamics in Liquids and Disordered Materials* (Springer-Verlag, New York, 2001).
14. G.B. DeMaggio, W.E. Frieze, D.W. Gidley, M. Zhu, H.A. Hristov, A.F. Yee, *Phys. Rev. Lett.* **78**, 1524 (1997).
15. K. Fukao, Y. Miyamoto, *Phys. Rev. E* **61**, 1743 (2000).
16. S. Napolitano, D. Prevosto, M. Lucchesi, P. Pingue, M. D'Acunto, P. Rolla, *Langmuir* **23**, 2103 (2007).
17. Z. Fakhraai, J.A. Forrest, *Science* **319**, 600 (2008).
18. S. Napolitano, C. Rotella, M. Wübbenhorst, *Acs Macro Lett.* **1**, 1189 (2012).
19. S. Napolitano, A. Pilleri, P. Rolla, M. Wübbenhorst, *Acs Nano* **4**, 841 (2010).
20. J.J. Hernandez, D.R. Rueda, M.C. Garcia-Gutierrez, A. Nogales, T.A. Ezquerra, M. Soccio, N. Lotti, A. Munari, *Langmuir* **26**, 10731 (2010).
21. D.R. Rueda, J.J. Hernandez, M.C. Garcia-Gutierrez, T.A. Ezquerra, M. Soccio, N. Lotti, A. Munari, J. Perlich, R. Serna, *Langmuir* **26**, 17540 (2010).
22. D.R. Rueda, A. Nogales, J.J. Hernandez, M.-C. Garcia-Gutierrez, T.A. Ezquerra, S.V. Roth, M.G. Zolotukhin, R. Serna, *Langmuir* **23**, 12677 (2007).
23. S. Napolitano, M. Wübbenhorst, *Nat. Commun.* **2**, 260 (2011).
24. A. Serghei, F. Kremer, *Macrom. Chem. Phys.* **209**, 810 (2008).
25. H.Y. Lu, W. Chen, T.P. Russell, *Macromolecules* **42**, 9111 (2009).
26. B. Frieberg, E. Glynos, G. Sakellariou, P.F. Green, *Acs Macro Lett.* **1**, 636 (2012).
27. B. Frieberg, E. Glynos, P.F. Green, *Phys. Rev. Lett.* **108**, (2012).
28. E. Glynos, B. Frieberg, H. Oh, M. Liu, D.W. Gidley, P.F. Green, *Phys. Rev. Lett.* **106**, (2011).
29. Z.H. Yang, Y. Fujii, F.K. Lee, C.H. Lam, O.K.C. Tsui, *Science* **328**, 1676 (2010).
30. D. Qi, Z. Fakhraai, J.A. Forrest, *Phys. Rev. Lett.* **101**, (2008).
31. C.R. Daley, Z. Fakhraai, M.D. Ediger, J.A. Forrest, *Soft Matter* **8**, 2206 (2012).
32. H.K. Nguyen, M. Labardi, S. Capaccioli, M. Lucchesi, P. Rolla, D. Prevosto, *Macromolecules* **45**, 2138 (2012).
33. J.E.G. Lipson, S.T. Milner, *Eur. Phys. J. B* **72**, 133 (2009).
34. V.M. Boucher, D. Cangialosi, H.J. Yin, A. Schonhals, A. Alegria, J. Colmenero, *Soft Matter* **8**, 5119 (2012).
35. J.C. Maxwell, *Philos. Trans. R. Soc. London* **157**, 49 (1867).
36. P.G. Debenedetti, F.H. Stillinger, *Nature* **410**, 259 (2001).
37. J.C. Dyre, *Rev. Mod. Phys.* **78**, 953 (2006).
38. L. Larini, A. Ottochian, C. De Michele, D. Leporini, *Nat. Phys.* **4**, 42 (2008).
39. K. Watanabe, T. Kawasaki, H. Tanaka, *Nat. Mater.* **10**, 512 (2011).
40. K. Ngai, *Relaxation and Diffusion in Complex Systems* (Springer, Berlin, 2011).
41. C. Bottcher, *Theory of Dielectric Polarization* (Elsevier Scientific Publishing Company, Amsterdam, 1973).
42. J. Runt, F.J. Fitzgerald, *Dielectric Spectroscopy of Polymeric Materials: Fundamentals and Applications* (American Chemical Society, 1997).
43. F. Kremer, A. Schonhals, *Broadband Dielectric Spectroscopy* (Springer, Berlin, 2003).
44. A. Schonhals, E. Schlosser, *Colloid Polym. Sci.* **267**, 125 (1989).
45. G. Tamman, G.Z. Hesse, *Anorg. Alleg. Chem.* **156**, 245 (1926).
46. G.S. Fulcher, *J. Am. Ceram. Soc.* **8**, 339 (1925).
47. H.Z. Vogel, *Phys. Z.* **22**, 645 (1921).
48. S. Havriliak, S. Negami, *Polymer* **8**, 161 (1967).
49. P. Bebin, R.E. Prud'homme, *Chem. Mater.* **15**, 965 (2003).
50. G. Blum, F. Kremer, T. Jaworek, G. Wegner, *Adv. Mater.* **7**, 1017 (1995).
51. A. Serghei, F. Kremer, *Rev. Sci. Instrum.* **77**, 116108 (2006).
52. E.U. Mapesa, M. Erber, M. Tress, K.J. Eichhorn, A. Serghei, B. Voit, F. Kremer, *Eur. Phys. J. ST* **189**, 173 (2010).
53. C. Rotella, S. Napolitano, M. Wübbenhorst, *Macromolecules* **42**, 1415 (2009).
54. M.C. Scott, D.R. Stevens, J.R. Bochinski, L.I. Clarke, *ACS Nano* **2**, 2392 (2008).
55. S. Capponi, S. Napolitano, N.R. Behrnd, G. Couderc, J. Hulliger, M. Wübbenhorst, *J. Phys. Chem. C* **114**, 16696 (2010).
56. M. Wübbenhorst, S. Capponi, S. Napolitano, S. Rozanski, G. Couderc, N.R. Behrnd, J. Hulliger, *Eur. Phys. J. ST* **189**, 181 (2010).
57. S. Capponi, S. Napolitano, M. Wübbenhorst, *Nat. Commun.* **3**, 1233 (2012).
58. M.W. den Otter, *Sensors, Actuators A: Phys.* **96**, 140 (2002).

59. S. Peter, S. Napolitano, H. Meyer, M. Wübbenhorst, J. Baschnagel, *Macromolecules* **41**, 7729 (2008).
60. P.S. Crider, M.R. Majewski, Z. Jingyun, H. Oukris, N.E. Israeloff, *Appl. Phys. Lett.* **91**, 013102 (2007).
61. M. Labardi, D. Prevosto, K.H. Nguyen, S. Capaccioli, M. Lucchesi, P. Rolla, *J. Vac. Sci. Technol. B* **28**, C4D11 (2010).
62. T.R. Albrecht, P. Grutter, D. Horne, D. Rugar, *J. Appl. Phys.* **69**, 668 (1991).
63. G. A. Schwartz, C. Riedel, R. Arinero, P. Tordjeman, A. Alegria, J. Colmenero, *Ultramicroscopy* **111**, 1366 (2011).
64. H.K. Nguyen, M. Labardi, M. Lucchesi, P. Rolla, D. Prevosto, *Macromolecules* **46**, 555 (2013).
65. C. Rotella, M. Wübbenhorst, S. Napolitano, *Soft Matter* **7**, 5260 (2011).
66. P. Scheidler, W. Kob, K. Binder, *Europhys. Lett.* **59**, 701 (2002).
67. P. Scheidler, W. Kob, K. Binder, *J. Phys. Chem. B* **108**, 6673 (2004).
68. D.S. Fryer, R.D. Peters, E.J. Kim, J.E. Tomaszewski, J.J. de Pablo, P.F. Nealey, C.C. White, W.L. Wu, *Macromolecules* **34**, 5627 (2001).
69. C.J. Vanoss, M.K. Chaudhury, R.J. Good, *Chem. Rev.* **88**, 927 (1988).
70. D. Labahn, R. Mix, A. Schoenhals, *Phys. Rev. E* **79**, 011801 (2009).
71. H. Yin, S. Napolitano, A. Schoenhals, *Macromolecules* **45**, 1652 (2012).
72. C. Rotella, S. Napolitano, S. Vandendriessche, V.K. Valev, T. Verbiest, M. Larkowska, S. Kucharski, M. Wübbenhorst, *Langmuir* **27**, 13533 (2011).
73. B. Vanroy, M. Wübbenhorst, S. Napolitano, *Acs Macro Lett.* **2**, 168 (2013).
74. O. Guiselin, *Europhys. Lett.* **17**, 225 (1991).
75. C.J. Durning, B. O'Shaughnessy, U. Sawhney, D. Nguyen, J. Majewski, G.S. Smith, *Macromolecules* **32**, 6772 (1999).
76. J.F. Douglas, H.M. Schneider, P. Frantz, R. Lipman, S. Granick, *J. Phys.: Condens. Matter* **9**, 7699 (1997).
77. S. Granick, *Eur. Phys. J. E* **9**, 421 (2002).
78. P. Linse, *Soft Matter* **8**, 5140 (2012).
79. C. Ligoure, L. Leibler, *J. Phys. (Paris)* **51**, 1313 (1990).
80. P. Gin, N. Jiang, C. Liang, T. Taniguchi, B. Akgun, S.K. Satija, M.K. Endoh, T. Koga, *Phys. Rev. Lett.* **109**, (2012).
81. S. Napolitano, M. Wübbenhorst, *Macromolecules* **39**, 5967 (2006).
82. K.L. Ngai, *J. Phys. Chem. B* **110**, 26211 (2006).
83. C. Bauer, R. Bohmer, S. Moreno-Flores, R. Richert, H. Sillescu, D. Neher, *Phys. Rev. E* **61**, 1755 (2000).
84. S. Srivastava, J.K. Basu, *Phys. Rev. Lett.* **98**, (2007).
85. J. Xu, D.W. Li, J. Chen, L. Din, X.L. Wang, F.F. Tao, G. Xue, *Macromolecules* **44**, 7445 (2011).
86. B.M.I. Flier, M. Baier, J. Huber, K. Muellen, S. Mecking, A. Zumbusch, D. Woell, *Phys. Chem. Chem. Phys.* **13**, 1770 (2011).
87. B.M.I. Flier, M.C. Baier, J. Huber, K. Mullen, S. Mecking, A. Zumbusch, D. Woll, *J. Am. Chem. Soc.* **134**, 480 (2012).
88. N.B. Tito, J.E.G. Lipson, S.T. Milner, *Soft Matter* **9**, 3173 (2013).
89. P.G. de Gennes, *Eur. Phys. J. E* **2**, 201 (2000).
90. D. Cangialosi, M. Wübbenhorst, J. Groenewold, E. Mendes, H. Schut, A. van Veen, S.J. Picken, *Phys. Rev. B* **70**, (2004).
91. V.M. Boucher, D. Cangialosi, A. Alegria, J. Colmenero, I. Pastoriza-Santos, L.M. Liz-Marzan, *Soft Matter* **7**, 3607 (2011).
92. D. Cangialosi, V.M. Boucher, A. Alegria, J. Colmenero, *J. Chem. Phys.* **135**, (2011).
93. V. M. Boucher, D. Cangialosi, A. Alegria, J. Colmenero, *Macromolecules* **45**, 5296 (2012).
94. D. Cangialosi, V.M. Boucher, A. Alegria, J. Colmenero, *Polymer* **53**, 1362 (2012).
95. M.S. McCaig, D.R. Paul, J.W. Barlow, *Polymer* **41**, 639 (2000).
96. A.W. Thornton, A.J. Hill, *Indust. Engin. Chem. Res.* **49**, 12119 (2010).
97. S. Napolitano, C. Rotella, M. Wübbenhorst, *Macromol. Rapid Commun.* **32**, 844 (2011).
98. P. Rittigstein, R.D. Priestley, L.J. Broadbelt, J.M. Torkelson, *Nat. Mater.* **6**, 278 (2007).
99. Z. Jiang, H. Kim, X. Jiao, H. Lee, Y.J. Lee, Y. Byun, S. Song, D. Eom, C. Li, M.H. Rafailovich, L.B. Lurio, S.K. Sinha, *Phys. Rev. Lett.* **98**, (2007).
100. G. Reiter, S. Napolitano, *J. Polym. Sci. Part B-Polym. Phys.* **48**, 2544 (2010).
101. G. Reiter, P.G. de Gennes, *Eur. Phys. J. E* **6**, 25 (2001).
102. G. Reiter, M. Hamieh, P. Damman, S. Sclavons, S. Gabriele, T. Vilmin, E. Raphael, *Nat. Mater.* **4**, 754 (2005).
103. D.R. Barbero, U. Steiner, *Phys. Rev. Lett.* **102**, 248303 (2009).
104. K.R. Thomas, A. Chenneviere, G. Reiter, U. Steiner, *Phys. Rev. E* **83**, (2011).
105. R.N. Li, A. Clough, Z. Yang, O.K.C. Tsui, *Macromolecules* **45**, 1085 (2012).
106. H. Richardson, I. Lopez-Garcia, M. Sferrazza, J.L. Keddie, *Phys. Rev. E* **70**, (2004).
107. H. Richardson, M. Sferrazza, J.L. Keddie, *Eur. Phys. J. E* **12**, S87 (2003).
108. T.N. Liang, Z.Q. Zhang, T. Li, X.Z. Yang, *Polymer* **45**, 1365 (2004).
109. C. Teng, Y. Gao, X. Wang, W. Jiang, C. Zhang, R. Wang, D. Zhou, G. Xue, *Macromolecules* **45**, 6648 (2012).
110. G.J. Fleer, M.A. Cohen Stuart, J.M.H.M. Scheutjens, T. Cosgrove, B. Vincent, *Polymer at Interfaces* (Chapman & Hall, London, 1998).
111. M.M. Santore, *Curr. Opin. Colloid Interface Sci.* **10**, 176 (2005).
112. R. Zajac, A. Chakrabarti, *Phys. Rev. E* **52**, 6536 (1995).
113. H.M. Schneider, P. Frantz, S. Granick, *Langmuir* **12**, 994 (1996).
114. T.Z. Fu, U. Stimming, C.J. Durning, *Macromolecules* **26**, 3271 (1993).
115. J. Baschnagel, K. Binder, *Macromolecules* **28**, 6808 (1995).

116. S. Peter, H. Meyer, J. Baschnagel, *J. Polym. Sci. Part B-Polym. Phys.* **44**, 2951 (2006).
117. S. Napolitano, M. Wübbenhorst, *J. Phys. Chem. B* **111**, 9197 (2007).
118. S. Napolitano, M. Wübbenhorst, *J. Phys. Chem. B* **111**, 5775 (2007).
119. Z. Fakhraai, J.A. Forrest, *Phys. Rev. Lett.* **95**, (2005).
120. S. Napolitano, V. Lupascu, M. Wübbenhorst, *Macromolecules* **41**, 1061 (2008).
121. R. Casalini, S. Capaccioli, M. Lucchesi, P.A. Rolla, M. Paluch, S. Corezzi, D. Fioretto, *Phys. Rev. E* **6404**, (2001).
122. S. Corezzi, D. Fioretto, P. Rolla, *Nature* **420**, 653 (2002).
123. J. Martin, C. Mijangos, A. Sanz, T.A. Ezquerra, A. Nogales, *Macromolecules* **42**, 5395 (2009).
124. A.A. Levchenko, P. Jain, O. Trofymuk, P. Yu, A. Navrotsky, S. Sen, *J. Phys. Chem. B* **114**, 3070 (2010).
125. S. Napolitano, M. Wübbenhorst, *J. Phys. Chem. B* **111**, 5775 (2007).
126. K. Fukao, T. Terasawa, Y. Oda, K. Nakamura, D. Tahara, *Phys. Rev. E* **84**, (2011).
127. K.L. Ngai, *Eur. Phys. J. E* **8**, 225 (2002).
128. C.J. Ellison, J.M. Torkelson, *Nat. Mater.* **2**, 695 (2003).
129. F. Dinelli, A. Ricci, T. Sgrilli, P. Baschieri, P. Pingue, M. Puttaswamy, P. Kingshott, *Macromolecules* **44**, 987 (2011).
130. F. Dinelli, T. Sgrilli, A. Ricci, P. Baschieri, P. Pingue, M. Puttaswamy, P. Kingshott, to be published in *J. Polym. Sci. Part B-Polym. Phys.*, DOI: 10.1002/polb.23310
131. T. Koga, N. Jiang, P. Gin, M.K. Endoh, S. Narayanan, L.B. Lurio, S.K. Sinha, *Phys. Rev. Lett.* **107**, (2011).
132. A. Serghei, M. Tress, F. Kremer, *J. Chem. Phys.* **131**, (2009).
133. S. Napolitano, M. Wübbenhorst, *Polymer* **51**, 5309 (2010).
134. C. Alvarez, I. Sics, A. Nogales, Z. Denchev, S.S. Funari, T.A. Ezquerra, *Polymer* **45**, 3953 (2004).
135. S. Napolitano, M. Wübbenhorst, *J. Non-Cryst. Solids* **353**, 4357 (2007).
136. S. Napolitano, M. Wübbenhorst, *J. Phys.: Condens. Matter* **19**, 205121 (2007).
137. P. Lunkenheimer, A. Pimenov, B. Schiener, R. Bohmer, A. Loidl, *Europhys. Lett.* **33**, 611 (1996).
138. U. Schneider, P. Lunkenheimer, R. Brand, A. Loidl, *J. Non-Cryst. Solids* **235**, 173 (1998).
139. C.B. Roth, J.M. Torkelson, *Macromolecules* **40**, 3328 (2007).
140. J.E. Pye, C.B. Roth, *Phys. Rev. Lett.* **107**, (2011).
141. J.A. Forrest, K. Dalnoki-Veress, J.R. Stevens, J.R. Dutcher, *Phys. Rev. Lett.* **77**, 2002 (1996).
142. S. Kim, C.B. Roth, J.M. Torkelson, *J. Polym. Sci. Part B-Polym. Phys.* **46**, 2754 (2008).
143. S. Kawana, R.A.L. Jones, *Phys. Rev. E* **63**, 021501 (2001).
144. S. Kim, J.M. Torkelson, *Macromolecules* **44**, 4546 (2011).
145. K. Paeng, S.F. Swallen, M.D. Ediger, *J. Am. Chem. Soc.* **133**, 8444 (2011).
146. J. Hintermeyer, A. Herrmann, R. Kahlau, C. Goiceanu, E.A. Rossler, *Macromolecules* **41**, 9335 (2008).
147. C. Zhang, Y. Guo, K. Shepard, R.D. Priestley, *J. Phys. Chem. Lett.* **4**, 431 (2013).
148. O. van den Berg, W.G.F. Sengers, W.F. Jager, S.J. Picken, M. Wübbenhorst, *Macromolecules* **37**, 2460 (2004).
149. R.D. Priestley, L.J. Broadbelt, J.M. Torkelson, K. Fukao, *Phys. Rev. E* **75**, (2007).
150. W.G.F. Sengers, O. van den Berg, M. Wübbenhorst, A.D. Gotsis, *Polymer* **46**, 6064 (2005).
151. K. Fukao, S. Uno, Y. Miyamoto, A. Hoshino, H. Miyaji, *Phys. Rev. E* **5**, 6405 (2001).
152. K. Fukao, S. Uno, Y. Miyamoto, A. Hoshino, H. Miyaji, *Phys. Rev. E* **6405**, (2001).
153. D. Labahn, R. Mix, A. Schonhals, *Phys. Rev. E* **79**, 9 (2009).
154. K. Fukao, S. Uno, Y. Miyamoto, A. Hoshino, H. Miyaji, *Phys. Rev. E* **64**, 11 (2001).
155. A. Serghei, M. Tress, F. Kremer, *Macromolecules* **39**, 9385 (2006).
156. A. Serghei, Y. Mikhailova, H. Huth, C. Schick, K.J. Eichhorn, B. Voit, F. Kremer, *Eur. Phys. J. E* **17**, 199 (2005).
157. P.K. Brazhnik, K.F. Freed, H. Tang, *J. Chem. Phys.* **101**, 9143 (1994).
158. C. Bauer, R. Richert, R. Bohmer, T. Christensen, *J. Non-Cryst. Solids* **262**, 276 (2000).
159. C.L. Soles, J.F. Douglas, W.L. Wu, H.G. Peng, D.W. Gidley, *Macromolecules* **37**, 2890 (2004).
160. C.J. Ellison, M.K. Mundra, J.M. Torkelson, *Macromolecules* **38**, 1767 (2005).
161. C. Kim, A. Facchetti, T.J. Marks, *Science* **318**, 76 (2007).
162. N. Hao, M. Bohning, H. Goering, A. Schonhals, *Macromolecules* **40**, 2955 (2007).
163. C. Housmans, M. Sferazza, S. Napolitano, in preparation.
164. J.E. Pye, C.B. Roth, *Phys. Rev. Lett.* **23**, 107 (2011) doi:10.1103/PhysRevLett.107.235701



**Simone Napolitano** obtained his MSc in Materials Science from the University of Pisa (2005) and, two years after, a PhD in Polymer Physics from KULeuven (Belgium), working with Michael Wübbenhorst. After an appointment as a postdoctoral researcher at the Research Foundation Flanders (FWO), in 2011 he joined the Université Libre de Bruxelles where he holds a faculty position and leads the laboratory of Polymers and Soft Matter Dynamics. His current research focuses on the molecular origin of the glass transition and the correlations between structure and dynamics in polymers and small molecules under nanoscopic confinement.



**Simona Capponi** studied Physics at the University of Perugia (Italy). Then she moved to Paris, where she worked for two years at Laboratoire de Physique des Solides (Paris). In 2012 she obtained her PhD degree from KULeuven (Belgium), where she investigated the structural dynamics of ultrathin films of H bonding liquids, obtained by physical vapour deposition. Currently, she is a postdoctoral researcher at the University College of Dublin (Ireland), in the group of J.H. Rice. Her research interests include surface characterization and spectroscopy of polymers and biomaterials.



Since 2010 **Bram Vanroy** is a PhD student in the division of Acoustics and Thermal Physics at KULeuven (Belgium) under the supervision of Michael Wübbenhorst. After first obtaining a degree in chemistry (2005-2010) he looked for a new challenge in the form of a PhD in the overlapping science of polymer physics and chemistry. His research interests are in the field of crystallization and adsorption of polymers under confinement and the formation of ultra-stable glasses.